

VOLUME 3 NUMBER 1 May 2014

**ISSN 2304-7445 (Print)
ISSN 2304-7461 (Online)**

Journal of Mechanical and Industrial Engineering Research



ELITE HALL PUBLISHING HOUSE

Journal of Mechanical and Industrial Engineering Research

ABOUT JOURNAL

The Journal of Mechanical and Industrial Engineering Research (J. mech. ind. eng. res. / JMIER) was first published in 2012, and is published semi-annually (May and November). JMIER is indexed and abstracted in: ProQuest, Electronic Journals Library, getCITED, ResearchBib, IndexCopernicus, Open J-Gate and JournalSeek. Since 2013, the JMIER has been included into the ProQuest, one of the leading full-text databases around the world.

The Journal of Mechanical and Industrial Engineering Research is an open access peer-reviewed international journal to be of interest and use to all those concerned with research in various fields of, or closely related to, mechanical and industrial engineering disciplines. Papers reporting original research or extended versions of already published conference/journal papers are all welcome. Papers for publication are selected through peer review to ensure originality, relevance, and readability.

Journal of Mechanical and Industrial Engineering Research

CONTENTS

- 1 **Publisher, Editor in Chief, Managing Editor and Editorial Board**
- 2 **EFFECT OF VARIOUS POROUS STRUCTURES ON THE MAGNETIC FLUID LUBRICATION OF A ROUGH INFINITELY LONG BEARING**
Jimit R. Patel and Gunamani Deheri
- 3 **Effect of WEDM machining parameters on material removal rate of tungsten carbide using DOE**
Nallavelli Ramesh, Sura Nagarjun
- 4 **Suitability of Illumination at the Engineering Computer Laboratory in Lyceum International Maritime Academy**
Kuster Kar C. Colina, Lemuel Dimaunahan, Carissa Mae Ramirez, Angelita M. Pagcaliwagan
- 5 **ANALYSIS FOR CONTROLLING BELT DEVIATION IN CONVEYOR SYSTEM**
Ankit Gupta
- 6 **Determination of Delamination and Surface Roughness for Machined Fiber Reinforced Plastics using Machine Vision**
G Dilli Babu, K. Sivaji Babu, B. Uma Maheswar Gowd
- 7 **EXPERIMENTAL ANALYSIS OF SPOT WELD GROWTH ON CARBON STEELS USING PNEUMATICS-DRIVEN 75KVA SPOT WELDER**
Nachimani Charde

Journal of Mechanical and Industrial Engineering Research

Publisher: Elite Hall Publishing House

Editor in Chief:

Dr. Mohammad Mohsin (India)
E-mail: mmohsinind@gmail.com

Managing Editor:

Dr. Jia Chi Tsou
Associate Professor, China University of Technology, Taiwan
E-mail: itsou.tw@yahoo.com.tw

Editorial Board:

Mr. Nachimani Charde
Department of Mechanical, Material and Manufacturing
Engineering, The University of Nottingham Malaysia Campus
E-mail: keyx9nac@nottingham.edu.my

Dr. Jake M. Laguador
Professor, Engineering Department
Lyceum of the Philippines University, Batangas City,
Philippines
E-mail: jakelaquador@yahoo.com

Dr. Sudhansu Sekhar Panda
Assistant Professor, Department of Mechanical Engineering
IIT Patna, India
Email: sspanda@iitp.ac.in

Dr. G Dilli Babu
Assistant Professor, Department of Mechanical Engineering,
V R Siddhartha Engineering College, Andhra Pradesh, India
Email: gdillibabu@gmail.com

Mr. Jimit R Patel
Research Scholar, Department of Mathematics,
Sardar Patel University, India
Email: patel.jimitphdmarch2013@gmail.com

Web: <http://jmier.elitehall.com>

ISSN 2304-7445 (Print)

ISSN 2304-7461 (Online)

EFFECT OF VARIOUS POROUS STRUCTURES ON THE MAGNETIC FLUID LUBRICATION OF A ROUGH INFINITELY LONG BEARING

Jimit R. Patel and Gunamani Deheri

Department of Mathematics, Sardar Patel University,
Vallabh Vidyanagar, Anand, Gujarat, India-388 120

Email: patel.jimitphdmarch2013@gmail.com, gm.deheri@rediffmail.com

ABSTRACT

An attempt has been made to study and analyze the performance characteristics of a magnetic fluid based rough porous long bearing considering the porous structure induced models of Kozeny- Carman and Irmay. The stochastically averaging of Christensen and Tonder has been adopted to account for transverse surface roughness. A magnetic fluid has been taken as the lubricant where in the magnitude of the magnetic field is described by an unusual form. The associated generalized Reynolds type equation is solved to obtain the pressure distribution resulting in the computation of load carrying capacity. The results presented in graphical form establish that the performance of the bearing system enhances considerably in the case of Kozeny- Carman model due to the magnetic fluid lubrication. It is needless to say that this article offers an additional degree of freedom from design point of view.

Keywords

Long Bearing, Roughness, Magnetic Fluid, Porous Structures.

INTRODUCTION

The classical theory of long bearing is a well established one (Majumdar, 2008; Hemrock, 1994; Szeri, 1998). The optimal design of a porous slider bearing with couple stress fluid lubrication was investigated by (Elasharkawy and Alyaqout, 2009). Here, an approach based on a sequential quadratic programming algorithm was proposed to minimize the friction.

(Kane and Bou-said, 2005) studied the non Newtonian effect and the effect of roughness in lubricated contacts. (Deheri et al., 2010) evaluated the effect of transverse surface roughness for an infinitely long hydrodynamic slider bearing. Here it was shown that the adverse effect of standard deviation associated with the roughness could be minimized by considering a proper combination of aspect ratio and ratio of outlet film thickness to the length of the bearing. (Deresses and Sinha, 2011) analyzed the thermal and roughness effects on different characteristics of a finite rough tilted pad slider bearing. It was established that the thermal and roughness combined effect on the load carrying capacity was more than due to the thermal effect for the both the roughness structures.(transverse as well as longitudinal). Recently, (Vakis and Polycarpou, 2013) presented a model of molecularly thin lubricant layer behaviour for rough sliding contact.

During the last decade the magnetic nano particles gained high importance because of their bio medical applications and rheological properties. These fluids tend to increase the viscosity of the lubricant resulting invariably in increased pressure. (Urreta et al., 2009) summarised the work carried out in the development of hydrodynamic journal bearing lubricated with a magnetic fluid. A finding of this paper has been used to develop active journal bearings. (Huang et al., 2011) considered the ferrofluid lubrication with an external magnetic field. The experimental results presented here indicated that the magnetic fluid turned in a good friction reduction performance.

(Patel and Deheri, 2011) investigated the combined effect of surface roughness and slip velocity on the magnetic fluid lubrication of a parallel plate porous slider bearing. It was found that the negatively

skewed roughness induced a relatively better performance especially, when the slip velocity was reduced. However, the friction remained unchanged. (Sukla and Deheri, 2011) considered the surface roughness effect on the behaviour of a magnetic fluid based porous secant shape slider bearing. Here, it was established that the negative effect of porosity and standard deviation could be reduced to a large extent by the positive effect of magnetization parameter in the case of negatively skewed roughness.

Here it has been sought to analyze the effect of various porous strictures on the magnetic fluid lubrication of a long porous rough bearing.

ANALYSIS

Figure 1 shows the geometry of the infinitely long bearing. The bearing system is infinite in Z direction. The slider moves with uniform velocity u in X direction. The length of the bearing is L and the breadth B is in Z direction.

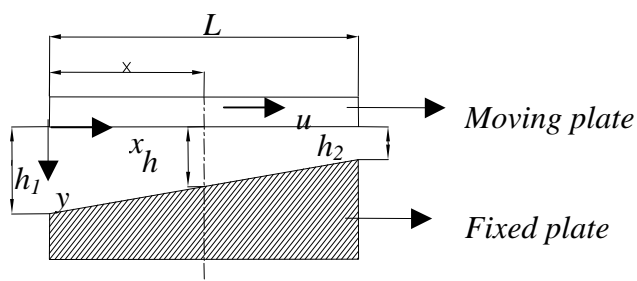


Figure 1. Geometry and configuration of the bearing system

It is taken into account that the lubricant film is isoviscous and incompressible and the flow is laminar.

It is taken that the bearing surfaces are transversely rough. According to the stochastic model of (Christensen and Tonder, 1969a; 1969b; 1970), the thickness $h(x)$ of the lubricant film is considered as

$$h(x) = \bar{h}(x) + h_s$$

where $\bar{h}(x)$ is the mean film thickness and h_s is the deviation from the mean film

thickness characterizing the random roughness of the bearing surfaces. h_s is described by the probability density function

$$f(h_s) = \begin{cases} (35/32c_1) \left(1 - (h_s^2/c_1^2)\right)^3, & -c_1 \leq h_s \leq c_1 \\ 0, & \text{elsewhere} \end{cases}$$

wherein c_1 is the maximum deviation from the mean film thickness. The mean α , the standard deviation σ and the parameter ε which is the measure of symmetry of the random variable h_s are defined and discussed in the study of (Christensen and Tonder, 1969a; 1969b 1970).

(Agrawal, 1986) considered the magnetic fluid lubrication effect by taking the magnetic field oblique to the stator. The effect of various forms of magnitude of the magnetic field has been discussed by (Prajapati, 1995). Following this discussion here, the magnitude of the magnetic field is considered to be

$$M^2 = kL^2(x/L)\sin(1 - (x/L))$$

where k is a suitably chosen constant from dimensionless point of view so as to produce a magnetic field of strength over 10^{-23} (Bhat and Deheri, 1995).

Under the usual assumptions of hydro magnetic lubrication (Bhat, 2003; Prajapati, 1995; Deheri et al., 2005) the Reynolds equation governing the pressure distribution is obtained as

$$d/dx \left(p - \left(\mu_0 \bar{\mu} M^2 / 2 \right) \right) = 6\mu u (h - \lambda h_2 / g(h))$$

(1)

where

$$g(h) = h^3 + 3h^2\alpha + 3(\sigma^2 + \alpha^2)h + 3\sigma^2\alpha + \alpha^3 + \varepsilon + 12\psi l_1$$

while μ_0 is the magnetic susceptibility, $\bar{\mu}$ is the free space permeability, μ is the lubricant viscosity and ψ is permeability of porous region, λ is a constant to be determined and l_1 is layer thickness.

The boundary conditions are

$p = 0$ at $x = 0$ and $x = L$

(2)

The following non dimension quantities are introduced

$$\begin{aligned}
 m &= (h_1 - h_2)/h_2, h = h_2(1 + m(1 - (x/L))), l^* = (l/l'), P = (h_2^3/\mu u \bar{L}^2) p, \mu^* = (h_2^3 k_{10} \bar{\mu}/\mu u), X = (x/L), \bar{L} = L/h_2, \\
 t &= (1 + m(1 - X)), \bar{\sigma} = \sigma/h_2, \bar{\alpha} = \alpha/h_2, \bar{\varepsilon} = \varepsilon/h_2^3, \bar{\psi} = (D_c^2 l_1)/h_2^3, \psi^* = (D_s^2 l_1)/h_2^3, a = 3\bar{\alpha}, b = 3(\bar{\alpha}^2 + \bar{\sigma}^2), \\
 c &= \bar{\varepsilon} + 3\bar{\sigma}^2 \bar{\alpha} + \bar{\alpha}^3 + (\bar{\psi} e^3 l^*/6(1-e)^2), J = (-2a^3 + 3(3)^{1/2} K + 9ab - 27c)^{1/3}, \\
 K &= (4a^3 c - a^2 b^2 - 18abc + 4b^3 + 27c^2)^{1/2}, J_1 = (J/3(2)^{1/3}) - ((2)^{1/3}(3b - a^2)/3J) - (a/3), Q = (J/6(2)^{1/3}), \\
 R &= ((3b - a^2)/3(2)^{2/3} J), J_2 = -2Q + 2R - (2a/3), J_3 = 4Q^2 + 4QR + 4R^2 + 2Q(a/3) - 2R(a/3) + (a^2/9), \\
 S &= J_1^2 - J_2 J_1 + J_3, A = J_1/S, B = -A, C = J_3/S, A_1 = 1/S, B_1 = -A_1, C_1 = J_2 - J_1/S, \\
 D &= \ln((1+m-J_1)/(1-J_1)), E = \ln(((1+m)^2 - J_2(1+m) + J_3)/(1-J_2 + J_3)),
 \end{aligned}$$

$$\begin{aligned}
 F &= \tan^{-1} \left(\frac{2m(4J_3 - J_2^2)^{1/2}}{\left((4J_3 - J_2^2) + (2(1+m) - J_2)(2 - J_2) \right)} \right), Q^* = (J^*/6(2)^{1/3}), \\
 G &= \left(\frac{J_2 B + 2C}{(4J_3 - J_2^2)^{1/2}} \right), H = \left(\frac{J_2 B_1 + 2C_1}{(4J_3 - J_2^2)^{1/2}} \right), C_1^* = J_2^* - J_1^*/S^*, \\
 \lambda &= (AD + (B/2)E + GF) / (A_1 D + (B_1/2)E + HF), P_1 = \ln \left(\frac{(t - J_1)}{(1 - J_1)} \right), \\
 P_2 &= \ln \left(\frac{(t^2 - J_2 t + J_3)}{(1 - J_2 + J_3)} \right), S^* = J_1^{*2} - J_2^* J_1^* + J_3^*, A^* = J_1^*/S^*, B^* = -A^*, C^* = J_3^*/S^*, \\
 P_3 &= \tan^{-1} \left(\frac{2m(1 - X)(4J_3 - J_2^2)^{1/2}}{\left((4J_3 - J_2^2) + (2t - J_2)(2 - J_2) \right)} \right), A_1^* = 1/S^*, B_1^* = -A_1^* \\
 w_1 &= \left(\frac{(1+m - J_1)}{(1 - J_1)} \right) D - 1, J_3^* = 4Q^{*2} + 4Q^* R^* + 4R^{*2} + 2Q^*(a/3) - 2R^*(a/3) + (a^2/9), \\
 I &= \tan^{-1} \left(\frac{2(1+m) - J_2}{(4J_3 - J_2^2)^{1/2}} \right) - \tan^{-1} \left(\frac{(2 - J_2)}{(4J_3 - J_2^2)^{1/2}} \right), \\
 N &= \ln \left(1 + \left(\frac{(2 - J_2)}{(4J_3 - J_2^2)^{1/2}} \right)^2 \right) - \ln \left(1 + \left(\frac{2(1+m) - J_2}{(4J_3 - J_2^2)^{1/2}} \right)^2 \right), \\
 w_2 &= \left(\frac{(4J_3 - J_2^2)^{1/2}}{m} \right) I - 2 + \left(\frac{2(1+m) - J_2}{2m} \right) E, w_1^* = \left(\frac{(1+m - J_1^*)}{(1 - J_1^*)} \right) D^* - 1, \\
 w_3 &= \left(\frac{2(1+m) - J_2}{2m} \right) I + \left(\frac{(4J_3 - J_2^2)^{1/2}}{4m} \right) N, H^* = \left(\frac{(J_2^* B_1^* + 2C_1^*)}{(4J_3^* - J_2^{*2})^{1/2}} \right), \\
 c^* &= \bar{\varepsilon} + 3\bar{\sigma} \bar{\alpha} + \bar{\alpha}^3 + (\psi^* (1 - (1 - e)^{2/3}) / (1 - e)), J^* = (-2a^3 + 3(3)^{1/2} K^* + 9ab - 27c^*)^{1/3}, \\
 K^* &= (4a^3 c^* - a^2 b^2 - 18abc^* + 4b^3 + 27c^{*2})^{1/2}, J_1^* = (J^*/3(2)^{1/3}) - ((2)^{1/3} (3b - a^2) / 3J^*) - (a/3), \\
 R^* &= ((3b - a^2) / 3(2)^{2/3} J^*), J_2^* = -2Q^* + 2R^* - (2a/3), G^* = \left(\frac{(J_2^* B^* + 2C^*)}{(4J_3^* - J_2^{*2})^{1/2}} \right), \\
 D^* &= \ln \left(\frac{(1+m - J_1^*)}{(1 - J_1^*)} \right), E^* = \ln \left(\frac{((1+m)^2 - J_2^*(1+m) + J_3^*)}{(1 - J_2^* + J_3^*)} \right), \\
 F^* &= \tan^{-1} \left(\frac{2m(4J_3^* - J_2^{*2})^{1/2}}{\left((4J_3^* - J_2^{*2}) + (2(1+m) - J_2^*)(2 - J_2^*) \right)} \right), \\
 \lambda^* &= (A^* D^* + (B^*/2)E^* + G^* F^*) / (A_1^* D^* + (B_1^*/2)E^* + H^* F^*), \\
 P_1^* &= \ln \left(\frac{(t - J_1^*)}{(1 - J_1^*)} \right), P_2^* = \ln \left(\frac{(t^2 - J_2^* t + J_3^*)}{(1 - J_2^* + J_3^*)} \right), \\
 P_3^* &= \tan^{-1} \left(\frac{2m(1 - X)(4J_3^* - J_2^{*2})^{1/2}}{\left((4J_3^* - J_2^{*2}) + (2t - J_2^*)(2 - J_2^*) \right)} \right), \\
 I^* &= \tan^{-1} \left(\frac{2(1+m) - J_2^*}{(4J_3^* - J_2^{*2})^{1/2}} \right) - \tan^{-1} \left(\frac{(2 - J_2^*)}{(4J_3^* - J_2^{*2})^{1/2}} \right), \\
 N^* &= \ln \left(1 + \left(\frac{(2 - J_2^*)}{(4J_3^* - J_2^{*2})^{1/2}} \right)^2 \right) - \ln \left(1 + \left(\frac{2(1+m) - J_2^*}{(4J_3^* - J_2^{*2})^{1/2}} \right)^2 \right), \\
 w_2^* &= \left(\frac{(4J_3^* - J_2^{*2})^{1/2}}{m} \right) I^* - 2 + \left(\frac{2(1+m) - J_2^*}{2m} \right) E^*, \\
 w_3^* &= \left(\frac{2(1+m) - J_2^*}{2m} \right) I^* + \left(\frac{(4J_3^* - J_2^{*2})^{1/2}}{4m} \right) N^*.
 \end{aligned}$$

(3)

Case 1: (A globular sphere model)

 A porous material is filled with globular particles (a mean particle size D_c) as shown in Figure A.

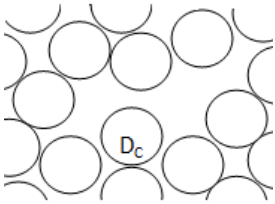


Figure A. Structure model of porous sheets given by Kozeny-Carman.

The Kozeny-Carman equation is a very useful relation in the field of fluid dynamics to calculate the pressure drop of a fluid flowing through a packed bed of solids. This model when applied gives better result in the case of laminar flow. The Kozeny-Carman equation mimics some experimental trends and hence serves as a quality control tool for physical and digital experimental results. The pressure gradient is assumed to be linear. In view of the discussion (Liu, 2009; Patel and Deheri, 2013) the use of Kozeny-Carman formula leads to

$$\psi = \left(D_c^2 e^3 \right) / \left(72(1-e)^2 \right) \left(l/l' \right)$$

where e is the porosity and l'/l is the length ratio. Under suitable assumptions this ratio turns out to be around 2.5 from experimental results. In that case the Kozeny-Carman formula becomes,

$$\psi = \left(D_c^2 e^3 \right) / \left(180(1-e)^2 \right)$$

Resorting to the non dimensional form of roughness term

$$g(\bar{h}) = \bar{t}^3 + 3\bar{t}^2\bar{\alpha} + 3\left(\bar{\sigma}^2 + \bar{\alpha}^2\right)\bar{t} + 3\bar{\sigma}^2\bar{\alpha} + \bar{\alpha}^3 + \bar{\varepsilon} + \frac{\bar{\psi}l^*e^3}{6(1-e)^2} \text{ and using the boundary conditions (2) the non}$$

dimensional form of the pressure distribution in the case of Kozeny- Carman, is found to be

$$P = \left(\mu^* / 2 \right) X \sin(1-X) + (6/m) \left(1/\bar{L} \right) \left[(\lambda A_1 - A)P_1 + (1/2)(\lambda B_1 - B)P_2 + (\lambda H - G)P_3 \right] (4)$$

The load carrying capacity of the bearing system is determined by

$$W = \left(h_2^3 / \mu u L^4 \right) w = \int_0^1 P dX$$

(5)

Thus, expression for the dimensionless load carrying capacity takes the

form

$$W = \left(\mu^* / 2 \right) (1 - \sin(1)) + (6/m) (1/\bar{L}) [(\lambda A_1 - A) w_1 + (1/2)(\lambda B_1 - B) w_2 + (\lambda H - G) w_3]$$

(6)

Case-2 :(A capillary fissures model)

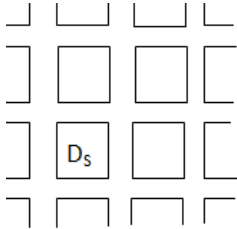


Figure B. Structure model of porous sheets given by Irmay.

Figure B, the model of porous sheets given by Irmay consists of three sets of mutually orthogonal fissures (a mean solid size D_s) and assuming no loss of hydraulic gradient at the junctions, (Irmay, 1955) derived the permeability,

$$\psi = \left(D_s^2 \left(1 - (1 - e)^{2/3} \right) \right) / (12(1 - e))$$

where e is the porosity.

Resorting to the boundary conditions (2) and making use of non dimensional form of roughness term

$$g(h^*) = A^3 + 3A^2\alpha + 3\left(\frac{-2}{\sigma} + \alpha^2 \right) A + 3\sigma \frac{-2}{\alpha + \alpha^3} + \varepsilon + \frac{\psi^* (1 - (1 - e)^{2/3})}{(1 - e)}$$

the dimensionless pressure distribution for Irmay

model is obtained as

$$P = \left(\mu^* / 2 \right) X \sin(1 - X) + (6/m) (1/\bar{L}) \left[(\lambda^* A_1^* - A^*) P_1^* + (1/2) (\lambda^* B_1^* - B^*) P_2^* + (\lambda^* H^* - G^*) P_3^* \right]$$

(7)

From Equation (5), the non-dimensional load carrying capacity is calculated as

$$W = \left(\mu^* / 2 \right) (1 - \sin(1)) + (6/m) (1/\bar{L}) \left[(\lambda^* A_1^* - A^*) w_1^* + (1/2) (\lambda^* B_1^* - B^*) w_2^* + (\lambda^* H^* - G^*) w_3^* \right] \quad (8)$$

RESULTS AND DISCUSSION

It is seen that Eq.(4;7) determines the non dimensional pressure distribution while the dimensionless load carrying capacity is calculated from Eq.(6;8). It is observed that the pressure increases by

$(\mu^*/2)X \sin(1-X)$ while the increase in load carrying capacity is $(\mu^*/2)(1-\sin(1))$ due to the magnetic fluid lubrication as compared to the case of traditional lubricants. In the absence of roughness this reduces to the study of a magnetic fluid based long bearing with porous structures. Further setting the magnetization parameter to be zero one gets the behaviour of a porous long bearing system. Besides, in the absence of porosity this turns to the discussion of long bearing (Basu et al., 2005). It is seen that the bearing system supports certain amount of load even if in the absence of flow unlike the case of a conventional lubricant. In fact, the increase in load carrying capacity can be at the best 8 % as compared to the case of conventional lubricant. Further, the expression for W is linear with respect to the magnetization parameter μ^* , which means that increasing values of magnetization would lead to increased load carrying capacity.

The variation of load carrying capacity for Case-1 is shown in Figures 2-15 while Figures 16-30 present the distribution of load carrying capacity in the case of Irmay's model. From the graphical representation one can conclude the following:

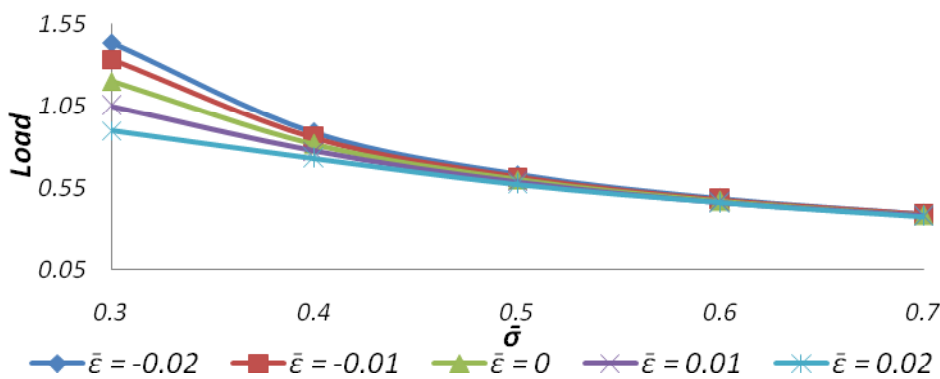


Figure 2. Variation of Load carrying capacity with respect to $\bar{\sigma}$ and $\bar{\epsilon}$.

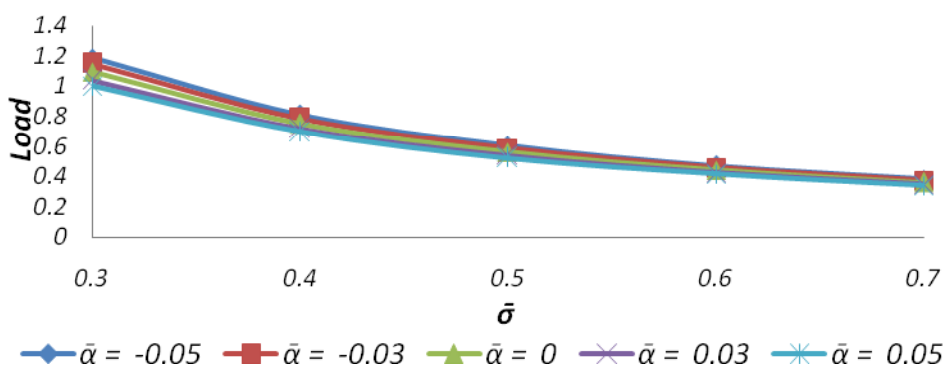


Figure 3. Variation of Load carrying capacity with respect to $\bar{\sigma}$ and $\bar{\alpha}$.

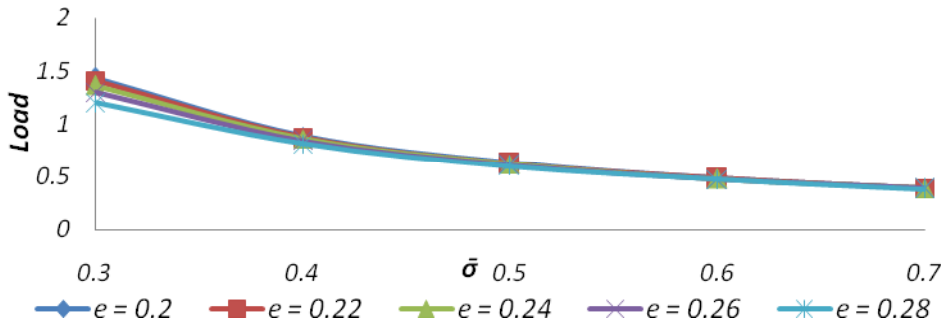


Figure 4. Variation of Load carrying capacity with respect to $\bar{\sigma}$ and e .

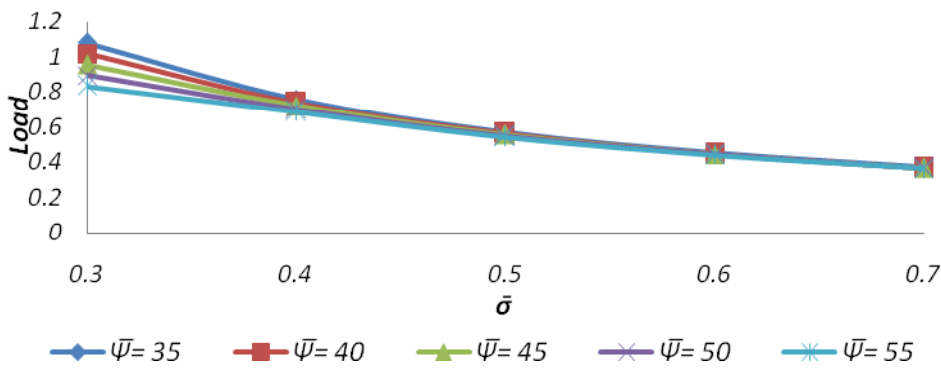


Figure 5. Variation of Load carrying capacity with respect to $\bar{\sigma}$ and $\bar{\psi}$.

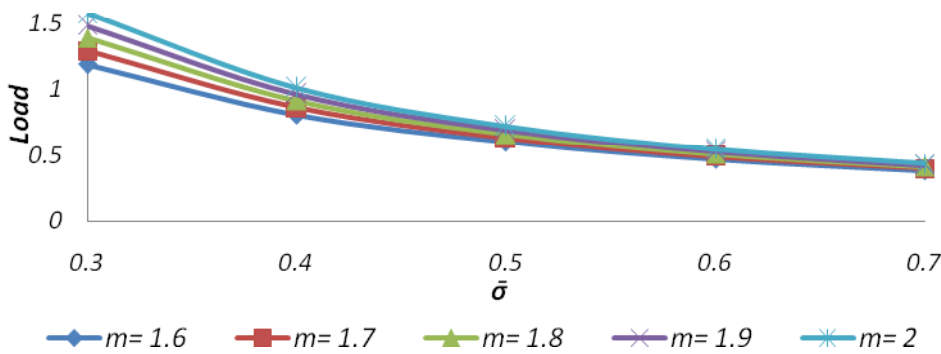


Figure 6. Variation of Load carrying capacity with respect to $\bar{\sigma}$ and m .

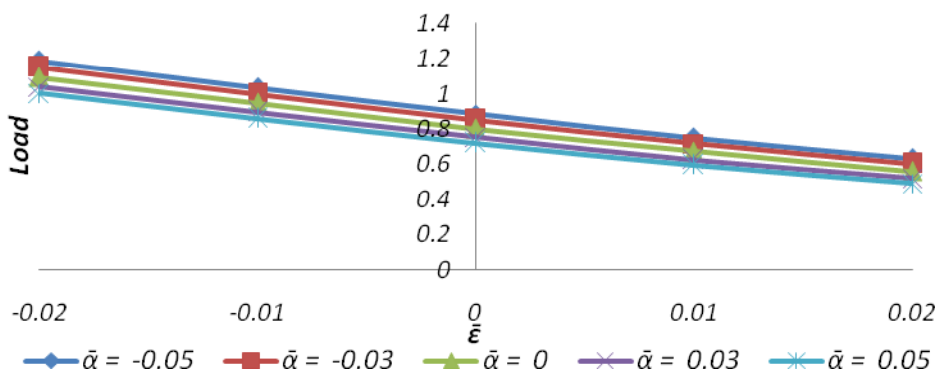


Figure 7. Variation of Load carrying capacity with respect to $\bar{\varepsilon}$ and $\bar{\alpha}$.

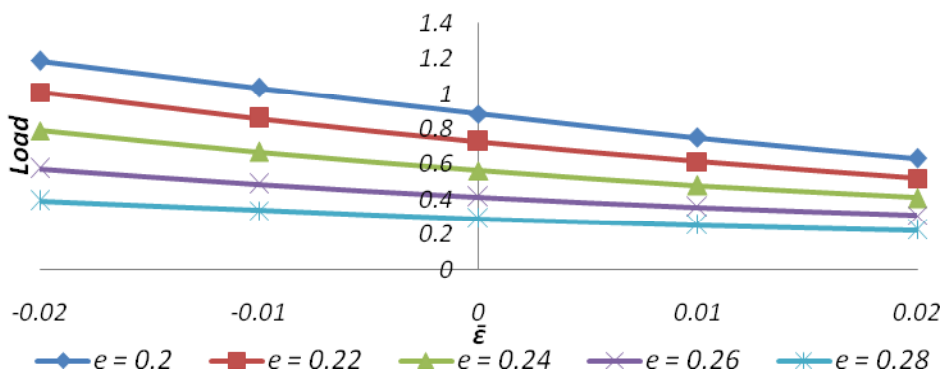


Figure 8. Variation of Load carrying capacity with respect to $\bar{\varepsilon}$ and e .

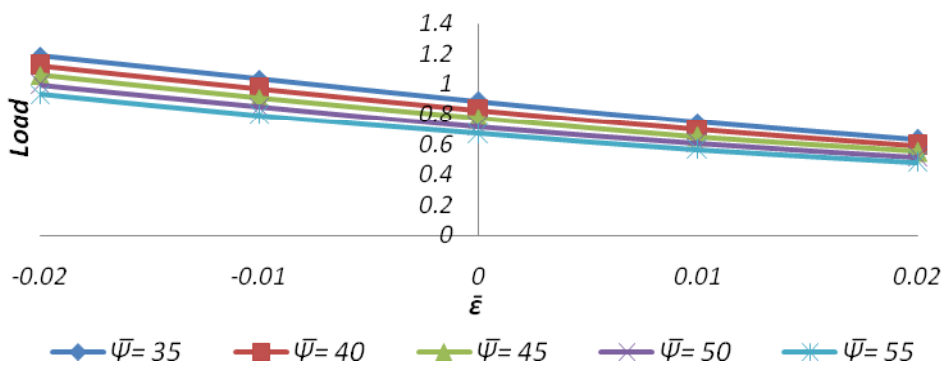


Figure 9. Variation of Load carrying capacity with respect to $\bar{\varepsilon}$ and $\bar{\psi}$.

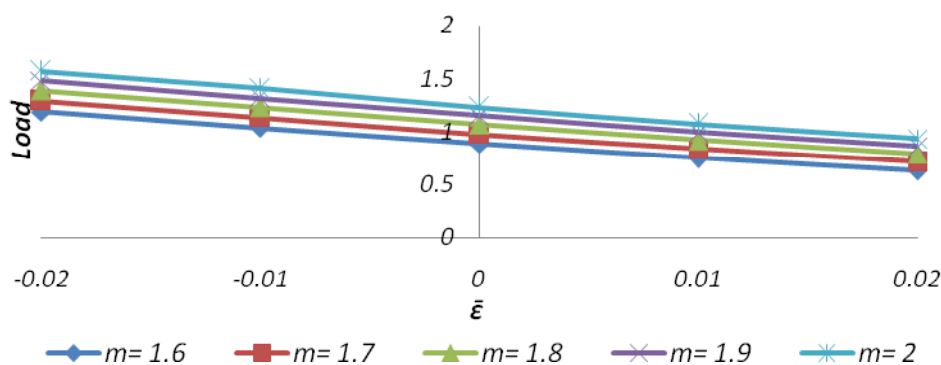


Figure 10. Variation of Load carrying capacity with respect to $\bar{\varepsilon}$ and m .

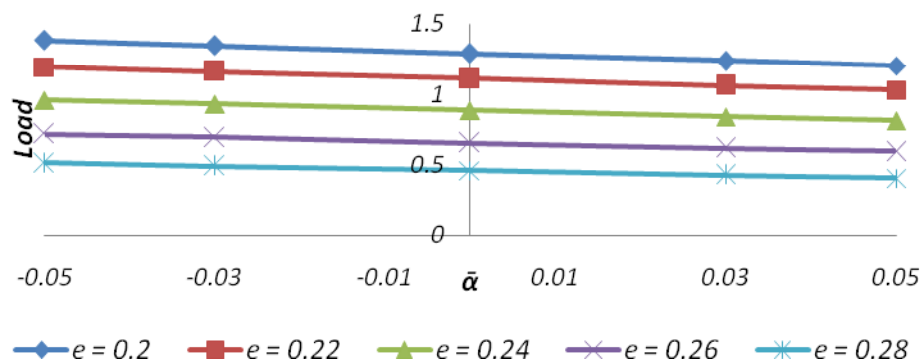


Figure 11. Variation of Load carrying capacity with respect to $\bar{\alpha}$ and e .

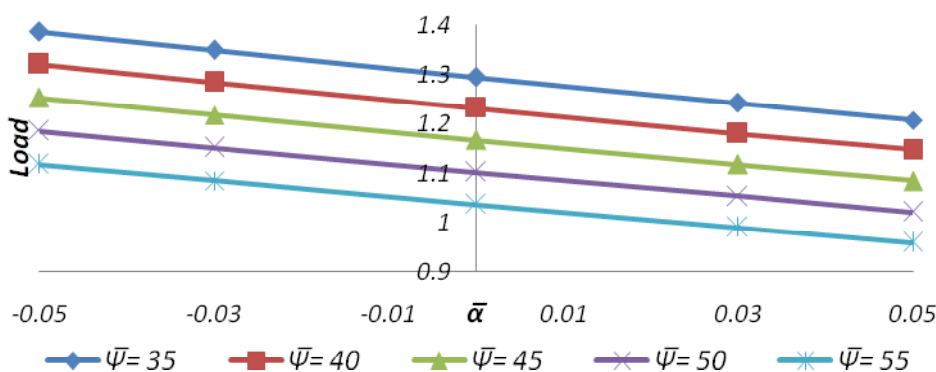


Figure 12. Variation of Load carrying capacity with respect to $\bar{\alpha}$ and $\bar{\psi}$.

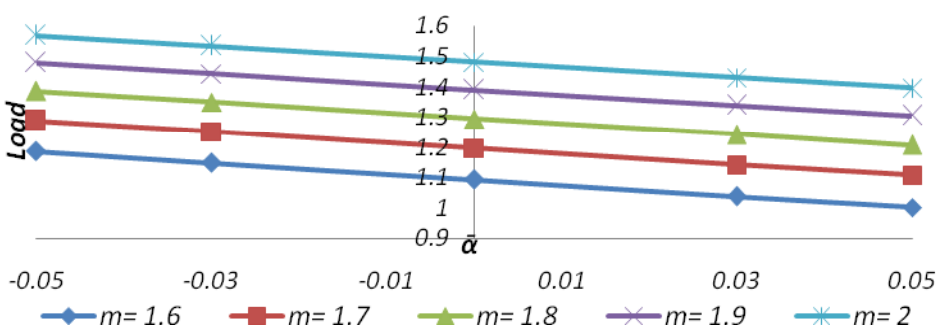


Figure 13. Variation of Load carrying capacity with respect to $\bar{\alpha}$ and m .

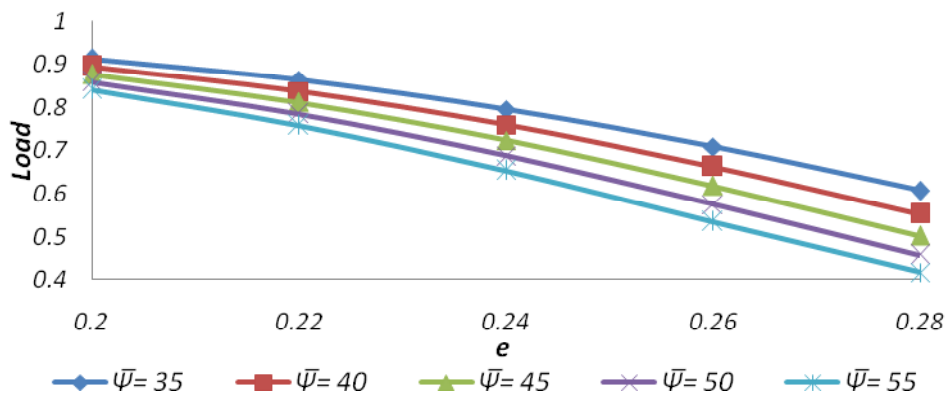


Figure 14. Variation of Load carrying capacity with respect to e and $\bar{\psi}$.

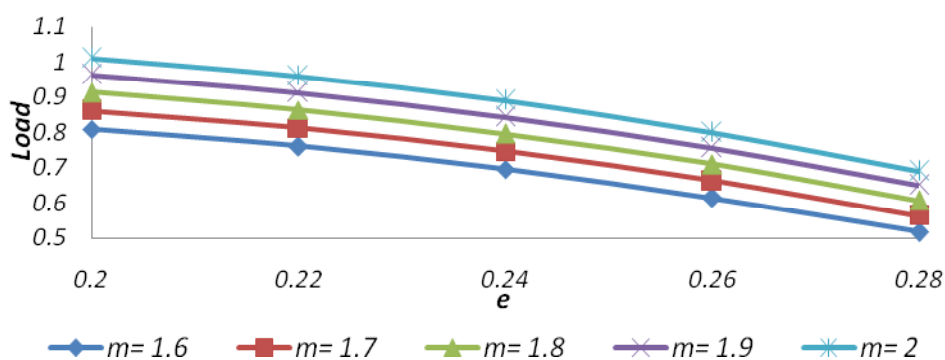


Figure 15. Variation of Load carrying capacity with respect to e and m .

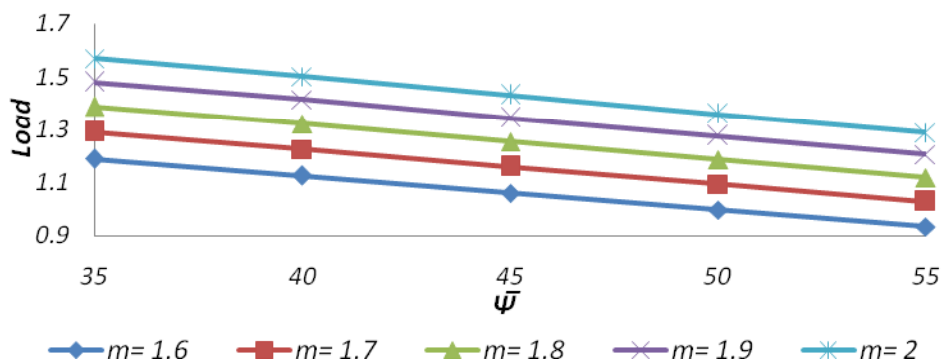


Figure 16. Variation of Load carrying capacity with respect to $\bar{\psi}$ and m .

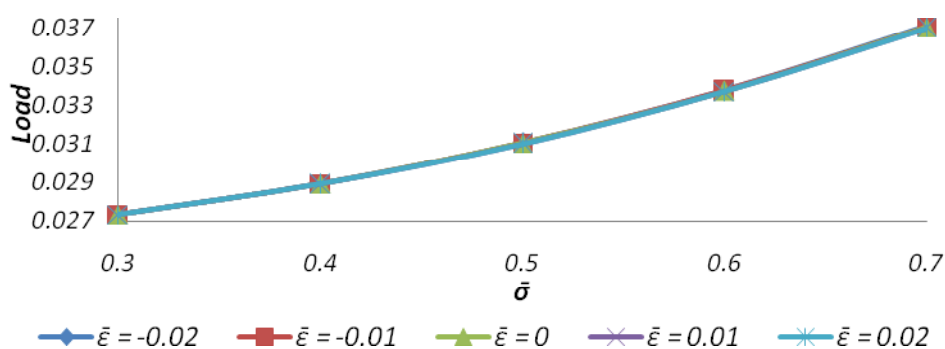


Figure 17. Variation of Load carrying capacity with respect to $\bar{\sigma}$ and $\bar{\varepsilon}$.

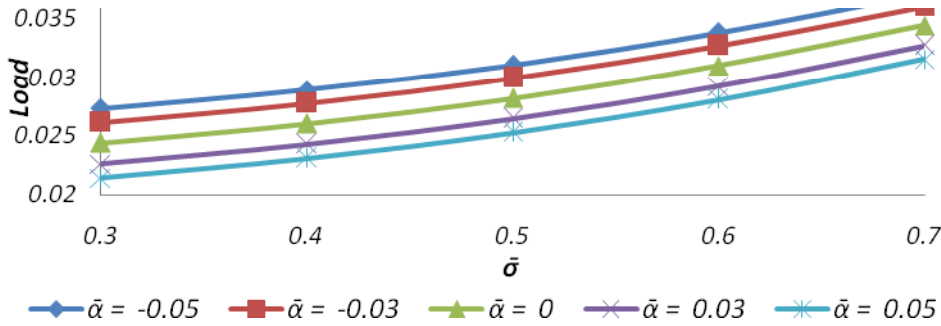


Figure 18. Variation of Load carrying capacity with respect to $\bar{\sigma}$ and $\bar{\alpha}$.

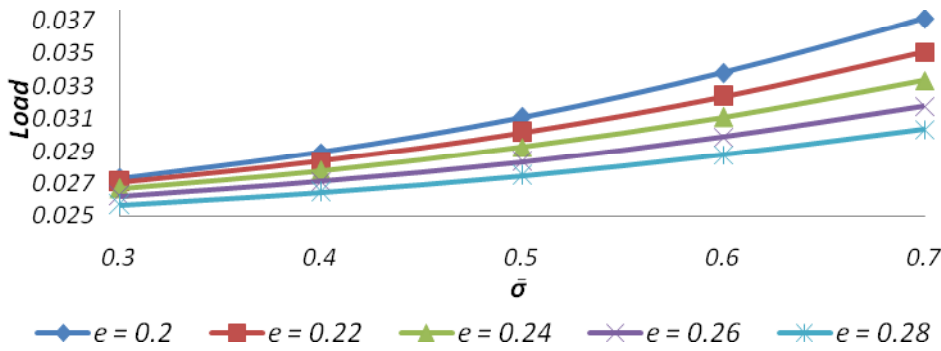


Figure 19. Variation of Load carrying capacity with respect to $\bar{\sigma}$ and e .

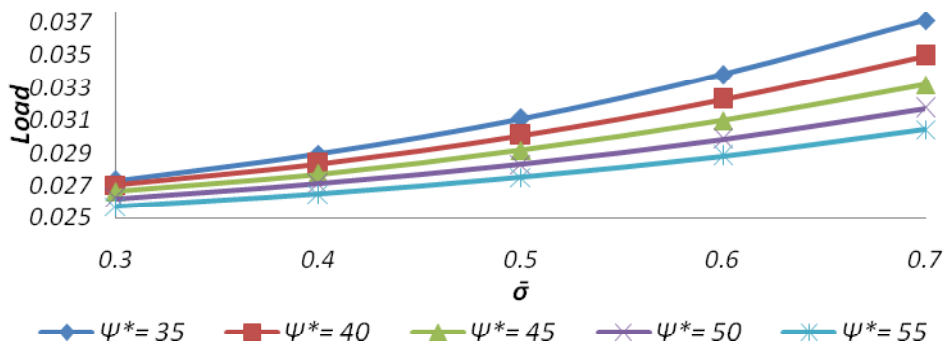


Figure 20. Variation of Load carrying capacity with respect to $\bar{\sigma}$ and ψ^* .

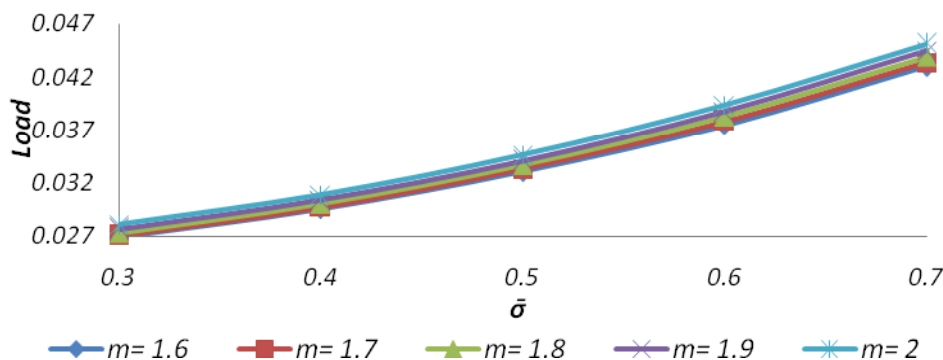


Figure 21. Variation of Load carrying capacity with respect to $\bar{\sigma}$ and m .

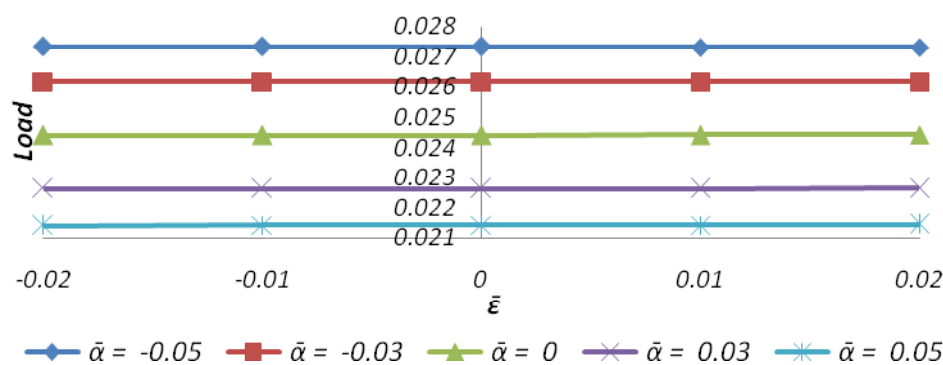


Figure 22. Variation of Load carrying capacity with respect to $\bar{\epsilon}$ and $\bar{\alpha}$.

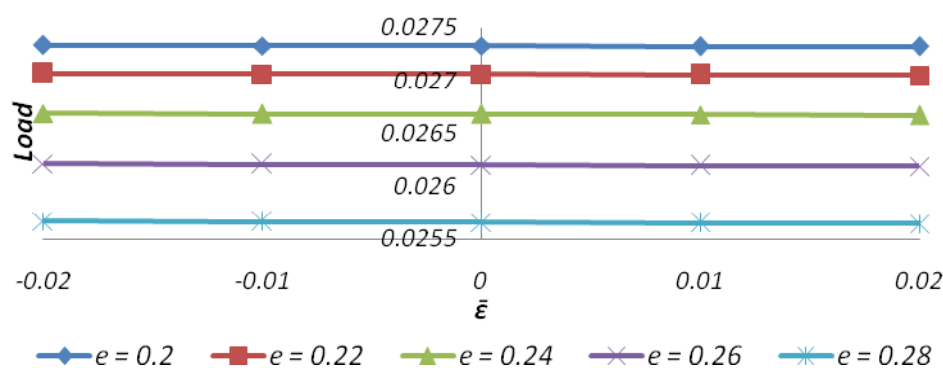


Figure 23. Variation of Load carrying capacity with respect to $\bar{\epsilon}$ and e .

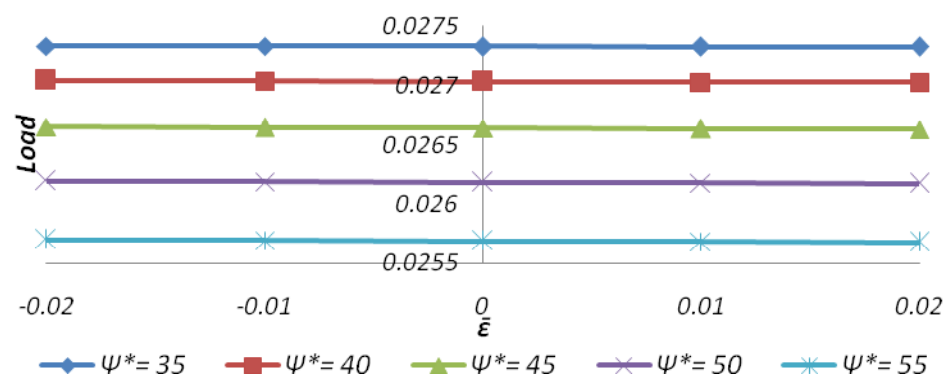
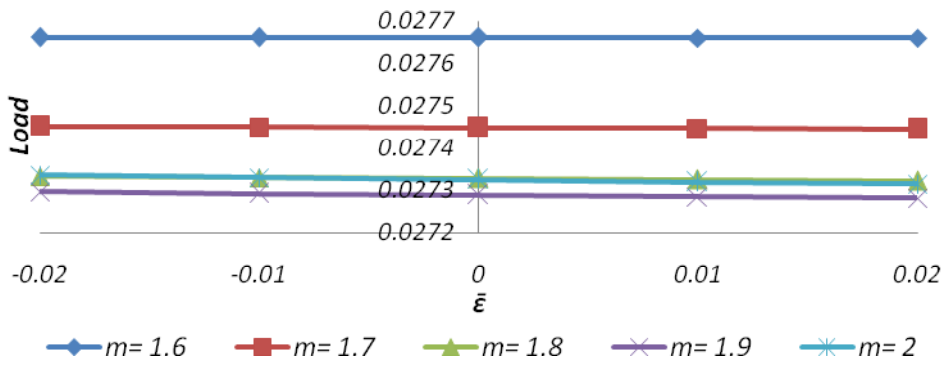
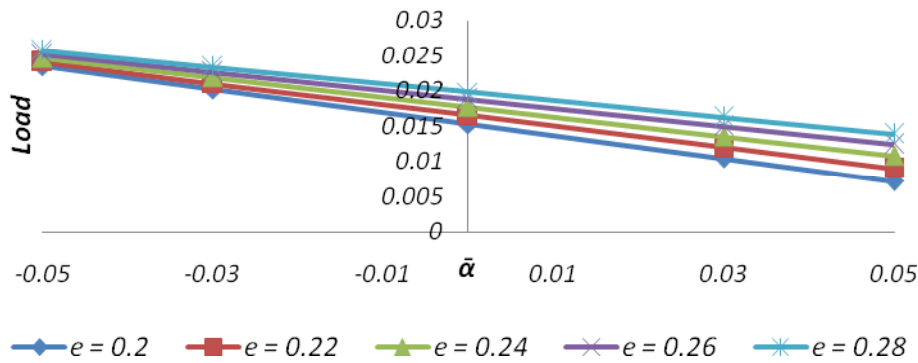
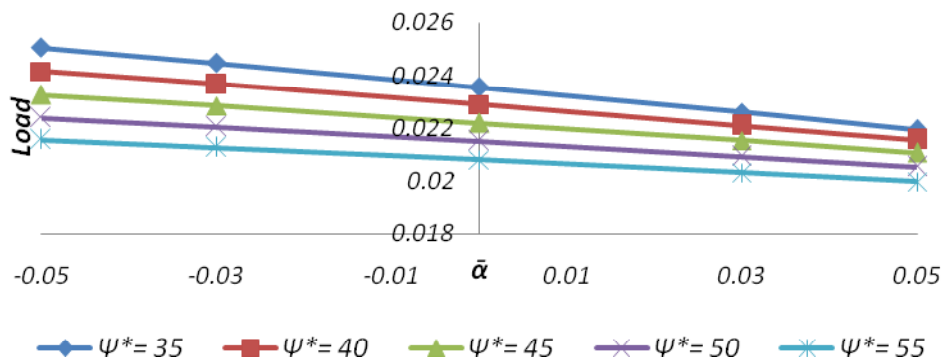


Figure 24. Variation of Load carrying capacity with respect to $\bar{\varepsilon}$ and ψ^* .

 Figure 25. Variation of Load carrying capacity with respect to $\bar{\varepsilon}$ and m .

 Figure 26. Variation of Load carrying capacity with respect to $\bar{\alpha}$ and e .

 Figure 27. Variation of Load carrying capacity with respect to $\bar{\alpha}$ and ψ^* .

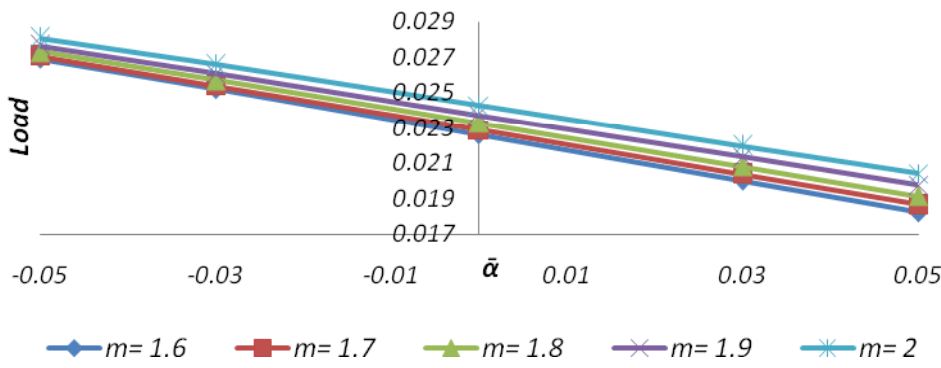


Figure 28. Variation of Load carrying capacity with respect to $\bar{\alpha}$ and m .

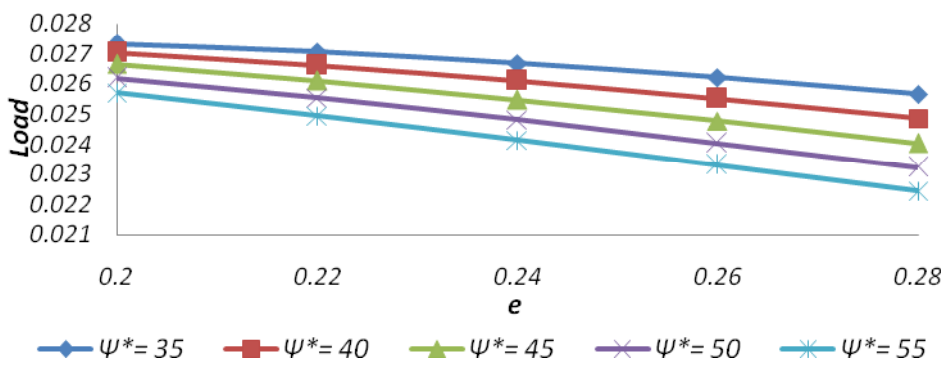


Figure 29. Variation of Load carrying capacity with respect to e and ψ^* .

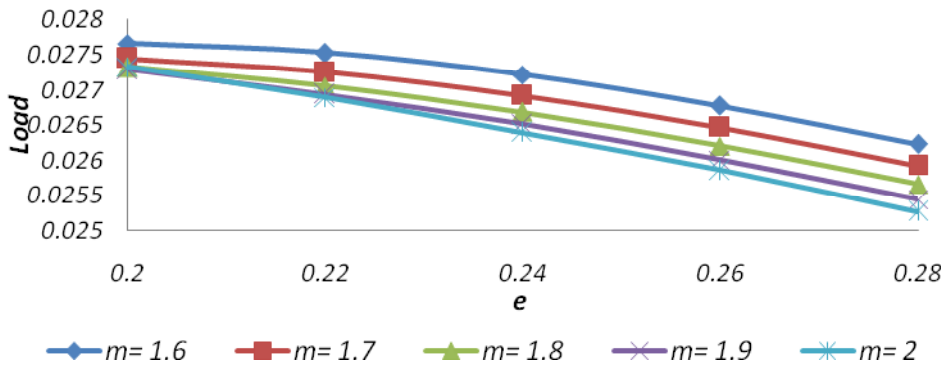


Figure 30. Variation of Load carrying capacity with respect to e and m .

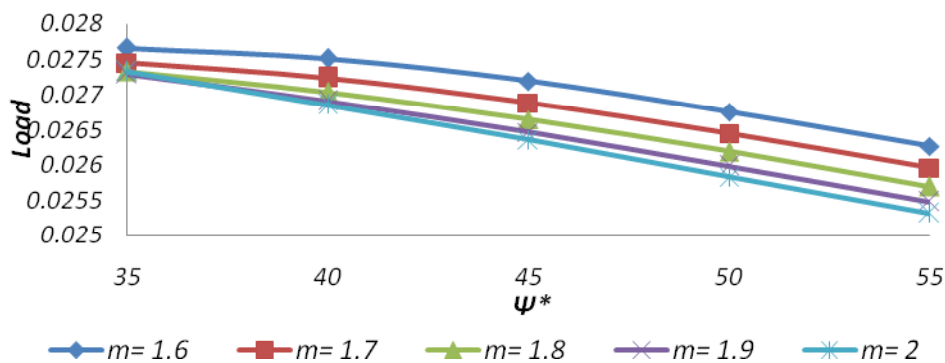


Figure 31. Variation of Load carrying capacity with respect to ψ^* and m .

The magnetization induces an increase in the load carrying capacity for both the cases. However, the magnetization effect is more impactable in the Kozeny-Carman's model, like the case of porous squeeze film in circular discs.

The load carrying capacity decreases due to the standard deviation associated with roughness. This is because the motion of the lubricant gets retarded by the roughness.

The negatively skewed roughness turns in an increase in the load carrying capacity, as does variance (-ve).

Interestingly, for a considerable range of standard deviation the effect of skewness on the load carrying capacity remains almost nominal.

For a suitable strength of the magnetic field the combined positive effect of negatively skewed roughness and variance (-ve) goes a long way in mitigating the adverse effect of porosity and standard deviation.

From designer's point of view the Kozeny- Carman's model may be little more suitable over the Irmay's model.

CONCLUSION

This article underlines that the roughness aspects deserve to be given due consideration while designing the bearing system even if suitable magnetic strength is in place. Besides, the compensation of the roughness induced adverse effect by the magnetic fluid lubrication appears to be more in the case of Kozeny-Carman's model at least in the case of negatively skewed roughness. Thus, Kozeny-Carman's

model scores over the Irmay's model for this type of bearing system from design point of view.

REFERENCES

- Agrawal, V.K. (1986). Magnetic fluid based porous inclined slider bearing. *WEAR*. 107: 133-139.
- Basu, S.K., Sengupta, S.N. and Ahuja, B.B. (2005). *Fundamentals of Tribology*. New Delhi: Prentice-Hall of India private limited.
- Bhat, M.V. (2003). *Lubrication with a Magnetic fluid*. India: Team Spirit (India) Pvt. Ltd.
- Bhat, M.V. and Deheri, G.M. (1995). Porous slider bearing with squeeze film formed by a magnetic fluid. *Pure and Applied Mathematika Sciences*. 39(1-2): 39-43.
- Christensen, H. and Tonder, K.C. (1969a). Tribology of rough surfaces: stochastic models of hydrodynamic lubrication. SINTEF. Report No.10:69-18.
- Christensen, H. and Tonder, K.C. (1969b). Tribology of rough surfaces: parametric study and comparison of lubrication models. SINTEF. Report No.22:69-18.
- Christensen, H. and Tonder, K.C. (1970). The hydrodynamic lubrication of rough bearing surfaces of finite width. ASME-ASLE Lubrication Conference. Cincinnati. OH. Paper no. 70-lub-7: October 12-15.
- Deheri, G.M., Andharia, P.I. and Patel, R.M. (2005). Transversely rough slider bearings with squeeze film formed by a magnetic fluid. *Int. J. of Applied Mechanics and Engineering*. 10(1): 53-76.
- Deheri, G.M., Changela, C.D., Patel, H.C. and Abhangi, N.D. (2010). Performance of an infinitely long transversely rough hydrodynamic slider bearing. *Advanced Tribology: Proceedings of CIST2008 & ITS-IFTtoMM2008*. 262-263.
- Deresse, G.A. and Sinha, P. (2011). THD analysis for finite slider bearing with roughness: special reference to load generation in parallel sliders. *Acta Mech*. 222: 1-15.
- Elsharkawy, A.A. and Alyaqout, S.F. (2009). Optimum shape design for surface of a porous slider bearing lubricated with couple stress fluid. *Lubrication Science*. 21(1): 1-12.
- Hamrock, B.J. 1994. *Fundamentals of Fluid film Lubrication*. New York: McGraw-Hill Inc.
- Huang, W., Shen, C., Liao, S. and Wang, X. (2011). Study on the ferrofluid lubrication with an external

magnetic field. *Tribology Lett.* 41: 145-151.

Irmay, S. (1955). Flow of liquid through cracked media. *Bull. Res. Council. Isr.* 5A(1): 84.

Kane, M. and Bou-Said, B. (2005). A study of roughness and Non-Newtonian effect in lubricated contacts. *Journal of Tribology.* 127(3): 575-581.

Liu, J. (2009). Analysis of a porous elastic sheet damper with a magnetic fluid. *Journal of Tribology.* 131: 0218011-15.

Majumdar, B.C. (2008). *Introduction to Tribology of Bearings.* New Delhi: S. Chand and Company Limited.

Patel, J R and Deheri, G M (2013). A comparison of porous structures on the performance of a magnetic fluid based rough short bearing, *Tribology in Industry* 35(3), 177-189.

Patel, N.D. and Deheri, G.M. (2011). Effect of surface roughness on the performance of a magnetic fluid based parallel plate porous slider bearing with slip velocity. *Journal of the Serbian Society for Computational Mechanics.* 5(1): 104-118.

Prajapati, B. L. (1995). *On Certain Theoretical Studies in Hydrodynamic and Electro-magneto hydrodynamic Lubrication.* Ph. D. Thesis: S.P. University. Vallabh Vidya- Nagar.

Shukla, S. and Deheri, G.M. (2011). Surface roughness effect on the performance of a magnetic fluid based porous secant shaped slider bearing. *Industrial Engineering Letters.* 1(2): 12-25.

Szeri, A.Z. (1998). *Fluid Film Lubrication: Theory and Design.* New York: Cambridge Univ. Press.

Urreta, H., Leicht, Z., Sanchez, A., Agirre, A., Kuzhir, P. and Magnac, G. (2009). Hydrodynamic bearing lubricated with magnetic fluids. *Journal of Physics: Conference series.* 149(1): Article ID 012113.

Vakis, A.I. and Polycarpou, A.A. (2013). An Advanced Rough Surface Continuum-Based Contact and Sliding Model in the Presence of Molecularly Thin Lubricant. *Tribology Letters.* 49(1): 227-238.

Effect of WEDM machining parameters on material removal rate of tungsten carbide using DOE

Nallavelli Ramesh¹, Sura Nagarjun²

¹Department of Mechanical Engineering,

SASTRA University,

Thanjavur, Tamilnadu,

India

rameshnallavelli1989@gmail.com

²Department of Mechanical Engineering,

NIT Warangal,

Warangal, AP,

India

suraarjun1086@gmail.com

ABSTRACT: Wire electrical discharge machining (WEDM) is a specialised thermal machining process capable of accurately machining parts with varying hardness or complex shapes, which have sharp edges that are very difficult to be machined by main stream machining processes. The main scope of this research work is to study the effects of various operational parameters like pulse on time (Ton), pulse off time (Toff), servo voltage (SV) and peak current (IP) on Material Removal Rate (MRR) of Tungsten carbide by WEDM. It is found that as Ton increases the Material Removal Rate increases, Toff increases Material Removal Rate (MRR) decreases, SV increases Material Removal Rate (MRR) decreases, IP increases Material Removal Rate (MRR) increases. The result of the experiment then was analysed using DESIGN EXPERT (DOE) software. This was done by using the TWO LEVEL FULL FACTORIAL technique and ANOVA analysis. In this study, randomization of the run order to be carried out and analysis sequences were carried out according to the run order by Design Expert software. Full factorial design of four factors with two levels each was conducted which consist of 16 runs. The machining responses that were analyzed is Material removal rate (MRR). All data obtained were then used as input to the Design Expert software for further analysis, according to steps outline for full factorial design. As Ton increased a projecting increment of MRR approximately 59.41% was observed.

KEYWORDS: WEDM, Ton, Toff, SV, IP, MRR, DOE, Two Level Full Factorial and ANOVA.

1. INTRODUCTION

In recent years, materials with unique metallurgical properties – such as tungsten carbide and its

composites, titanium based alloys, nickel based alloys, tool steels, stainless steels, hardened steels and other super alloys – have been developed to meet the demands of extreme applications. While these materials are harder, tougher, less heat sensitive and/or more resistant to corrosion and fatigue, they are more difficult to machine [1]. Difficult-to-cut materials have been widely used these days not only in the aerospace industry but also in the public welfare industry [2]. Wire Electrical Discharge machining (WEDM) is a nontraditional, thermoelectric process which erodes material from the work piece by a series of discrete sparks between workpiece and electrode that immersed in a dielectric medium [3]. Sometimes called travelling wire EDM electrical discharge wire cutting is a process that is similar in configuration to bandsawing except in the case of WEDM the “saw” is a wire electrode of small diameter. Material removal is affected as a result of spark erosion as the wire electrode is fed through the workpiece. The electrode wire is used only once, then discarded because the wire loses its form after one pass through the workpiece. A steady stream of deionized water or other fluid is used to cool the workpiece and electrode wire and to flush the cut area. [4].

Wire electrical discharge machining (WEDM) is a specialised thermal machining process capable of accurately machining parts with varying hardness or complex shapes, which have sharp edges that are very difficult to be machined by main stream machining processes. This practical technology of the WEDM process is based on the conventional EDM sparking phenomenon utilizing the widely accepted non-contact technique for the material removal [5]. WEDM is considered as a highly précised and accurate. It is one of the most popular processes in conventional machining.[6] Hewidy et al.[7] applied response surface methodology (RSM) for modeling of machining parameters WEDM of Inconel 601. They modeled volu-metric material removal rate, wire wear rate and surface roughness according to variation of peak currant, pulse on time, wire tension and water pressure. Liao et al. [8] proposed an approach of determining the parameter settings based on the Taguchi quality design method and the analysis of variance. The results showed that the MRR and SF are easily influenced by the table feed rate and pulse on-time, which can also be used to control the discharging frequency for the prevention of wire breakage. Lok and Lee [9] compared the machining performance in terms of MRR and surface finish through observations obtained by processing of two advanced ceramics under different cutting conditions using WEDM. This methodology was used by some researchers for statistical methods and full factorial design of experiments has been used for machinability [10] and surface roughness [11]. J.S. Senthikumar et al.[12] conducted the experiments as per full factorial design of experiments under dry cutting condition in machining i.e. finish turning and facing of Inconel 718, and optimised the machining parameters on surface roughness & flank wear using Taguchi technique. M. Kaladhar et al.[13] determined the best levels of machining parameters such as cutting speed, feed, depth of cut and nose radius to obtain the minimum surface roughness during turning of AISI 202 austenitic stainless steel using full factorial design of experiment.

Design of experiment (DOE) is series of tests in which purposeful changes are made to the input variables of a process or system so that the reasons for change in the output responses can be observed and identified. Advantages of DOE are as follows:

1. Numbers of trials is significantly reduced.
2. Important decision variables which control and improve the performance of the product or the process can be identified.
3. Optimal setting of the parameters can be found out.
4. Qualitative estimation of parameters can be made.
5. Experimental error can be estimated.
6. Inference regarding the effect of parameters on the characteristics of the process can be made.

2. EXPERIMENT PROCEDURE:

The experiment is carried out on the work piece material of Tungsten Carbide. The Tungsten carbide plate of 125mm x 100mm x 25mm size was used. Tungsten carbide is composed of tungsten, titanium, tantalum and vanadium carbides in various amounts that on sintered or cemented in a matrix using mostly cobalt as binder or nickel if corrosion resistance is required[9]. Brass wire of 0.25 mm is used as tool material. The programme was made for cutting operation of the work piece and a profile of 10mm diameter circle was cut. Each set of experiments are performed at room temperature in a narrow temperature range of $32\pm 2^{\circ}\text{C}$. Some of the parameters like pulse on time, pulse off time, servo voltage and peak current are taken according to the settings of machine [14].

2.1 EXPERIMENTAL DESIGN STRATEGY

Two level full factorial designs will help us to screen many factors to discover the vital few, and perhaps how they interact. Here the data you will now analyze comes from Douglas Montgomery's textbook, design and Analysis of Experiments, published by John Wiley and Sons.

In the two levels Full Factorial method the results of the experiments are analyzed to achieve one or more of the following objectives:

- a. To establish the best or the optimum condition for a product or process.
- b. To estimate the contribution of individual parameters and interactions.
- c. To estimate the machining characteristics under the optimum condition

The optimum condition is identified by studying the main effects of each of the parameters. The main effects indicate the general trends of influence of each parameter. The knowledge of contribution of individual parameters is a key in deciding the nature of control to be established on a production process. The analysis of variance (ANOVA) is the statistical treatment most commonly applied to the results of the experiments in determining the percent contribution of each parameter against a stated level of confidence. Study of ANOVA table for a given analysis helps to determine which of the parameters need control. Given below a flow chart in Fig.1 steps outlining of the analysis undertaken.

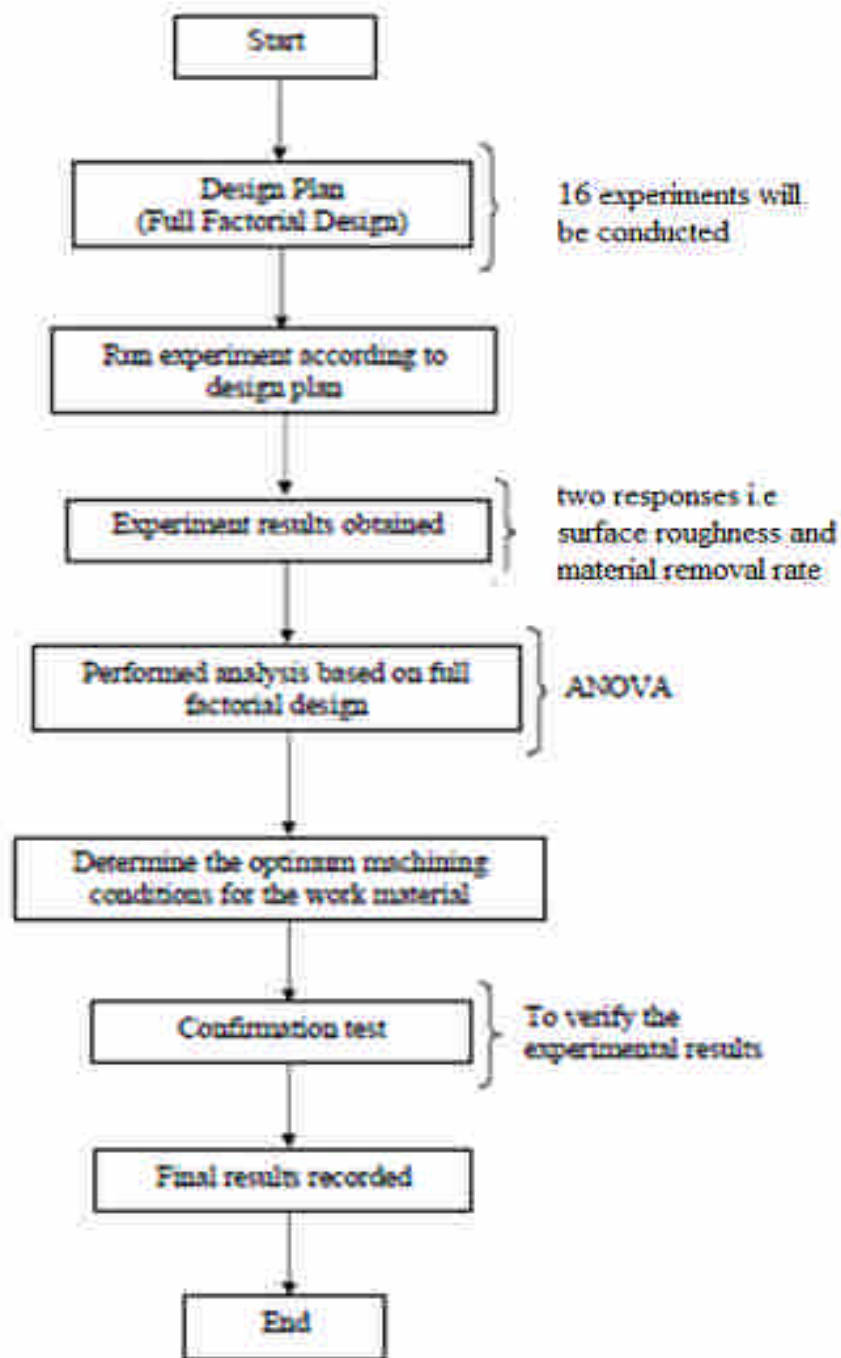


Fig. 1: Flow chart outlining the analysis steps undertaken

In this study, randomization of the run order to be carried out and analysis sequences were carried out according to the run order by Design Expert software. Full factorial design of four factors with two levels each was conducted which consist of 16 runs. The machining responses that were analyzed were surface roughness (Ra), and **Material removal rate (MRR)**.

All data obtained were then used as input to the Design Expert software for further analysis, according to steps outline for full factorial design. The overall experimental results corresponding to each run generated by the software are shown below Table1.

Table1:Design Experiment software results

Std	Run	Factor 1 A:A.Pulse on. µs	Factor 2 B:B.Pulse off. µs	Factor 3 C:C.Servo v. v	Factor 4 D:D.Peak Cur. A	Response 1 R1.Surface µm	Response 2 R2.Material R. mm2/min
15	1	105.00	63.00	80.00	230.00	1.37	0.0042
5	2	105.00	39.00	80.00	50.00	1.48	0.0069
11	3	105.00	63.00	5.00	230.00	1.72	0.0055
9	4	105.00	39.00	5.00	230.00	1.97	0.011
2	5	126.00	39.00	5.00	50.00	2.65	0.0202
13	6	105.00	39.00	80.00	230.00	1.7	0.00774
14	7	126.00	39.00	80.00	230.00	2.35	0.0174
7	8	105.00	63.00	80.00	50.00	1.7	0.0036
1	9	105.00	39.00	5.00	50.00	1.62	0.0091
10	10	126.00	39.00	5.00	230.00	2.78	0.0232
8	11	126.00	63.00	80.00	50.00	2.2	0.0086
4	12	126.00	63.00	5.00	50.00	2.35	0.012
6	13	126.00	39.00	80.00	50.00	2.29	0.0154
12	14	126.00	63.00	5.00	230.00	2.55	0.0134
3	15	105.00	63.00	5.00	50.00	1.68	0.0053
16	16	126.00	63.00	80.00	230.00	2.1	0.0098

3. ANALYSIS OF RESULTS

As mentioned earlier, Design Expert software was used to analyze the results obtained in order to identify the significant factors and interactions between the factors under studied. Analysis of variance (ANOVA) table is commonly used to summarize the experimental results. These tables conclude information of analysis of variance and case statistics for further interpretation. In this section, all the analysis was presented in normal probability plot, main effect plot and interaction plot for the dependent parameters that significant to the responses. The interpretations were done unilaterally, meaning that ANOVA analysis for all three responses was done separately at one time.

3.1 Analysis Results for Material Removal Rate

Material removal rate (MRR) in WEDM processes is an important factor because of its vital effect on the production cost.

Table 2 indicates the final analysis of ANOVA for material removal rate (MRR)

Table 2: ANOVA for Material Removal Rate, MRR

Source	Sum of Squares	Degree of freedom	Mean square	F-Value	Contribution (%)
A. Pulse on time	2.77E-004	1	2.77E-004	96.10	59.41
B. Pulse off time	1.473E-004	1	1.473E-004	50.95	31.50
C. Servo voltage	4.245E-005	1	4.245E-005	14.69	9.082
Residual	3.468E-005	12	2.890E-006		
Total		15		161.74	99.99

Based on Figure 3.1, the significant factors were observed better in the normal probability plot of the standardized effects. As displayed in the Figure 3.1, the significant factors highlighted were pulse on time (Ton) and pulse off time (Toff) and servo voltage (SV) which denoted as A and B and C respectively. In order to have clearer observation and better understanding of the response, the main effect plot is available. However, in this software, only the significant effect is displayed in the main effect graph and not the insignificant factors.

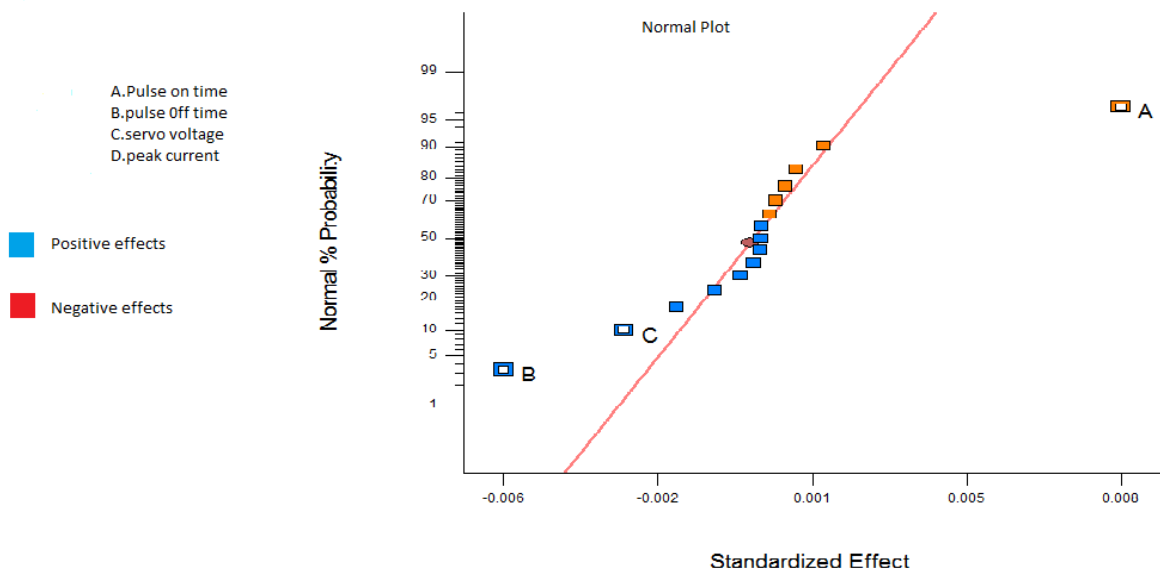


Fig 3.1: Normal Probability plot for MRR

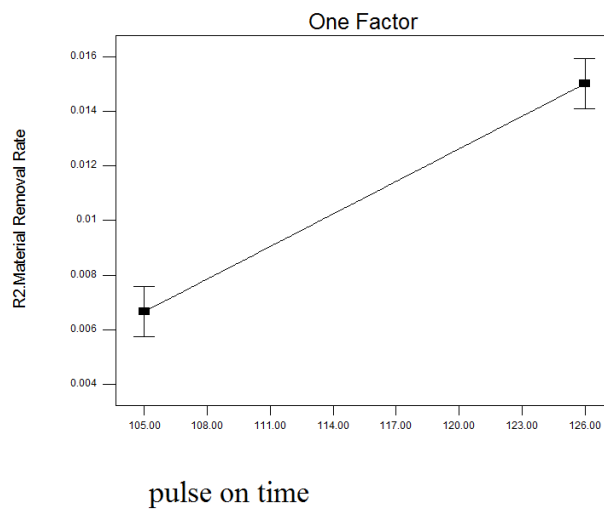


Fig 3.2: Plot between MRR and pulse on time

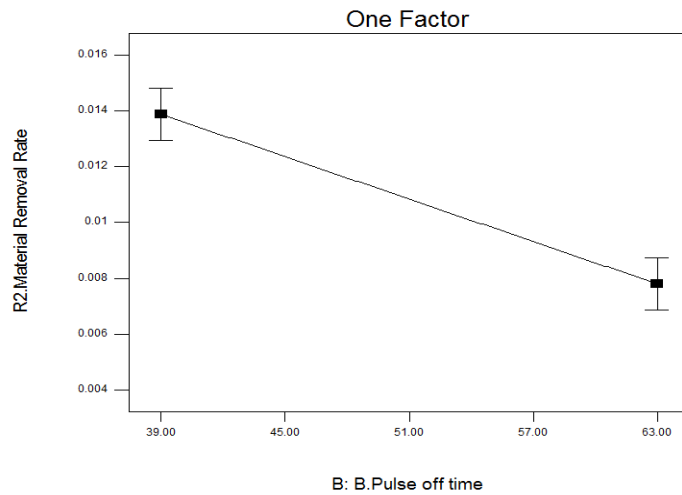


Fig 3.3: Plot between MRR and pulse off time

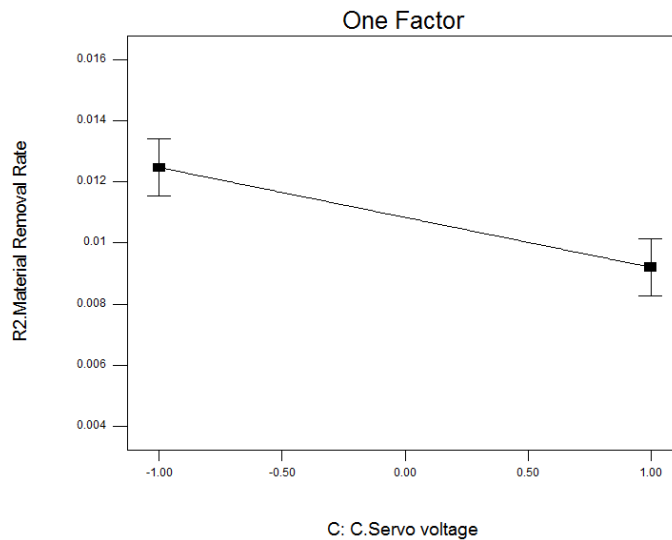


Fig 3.4: Plot between MRR and servo voltage

3.2 Main effects Plot for MRR

From the main effects plot, it was clearly showed that whenever T_{on} increased from 105 μs to 126 μs , the value of MRR also increased dramatically as shown in Fig 3.2. The projecting increment of MRR was approximately 59.41%. Meanwhile, a reverse result was observed for T_{off} effect as the graph showed in Fig 3.3 that MRR decreased when T_{off} increased from 39 μs to 63 μs . The decrement of MRR was about 31.50% when T_{off} setting was at 63 μs . Meanwhile, a reverse result was observed for SV effect as the graph showed in Fig 3.4 that MRR decreased when SV increased from 5 volt to 80 volt. The

decrement of MRR was about 9.082% when SV setting was at 80 volt. Based on the ANOVA analysis, TON and SV were affecting the MRR individually.

The mathematical model for MRR was also developed by ANOVA analysis in order to identify the relationship between independent variables, namely, Ton and MRR. The following equation is the final empirical models in terms of coded and factors and actual factors for MRR respectively. This equation was generated by the Design Expert after the transformation had been carried out.

Final equation in terms of coded factors

$$R2. \text{ Material Removal Rate} = +0.011 + 4.166E-003 * A - 3.034E-0.003 * B - 1.629-003 * C.$$

Final equation interms of Actual factors

$$R2. \text{ Material Removal Rate} = - 0.020256 + 3.96786E-004 * A. \text{Pulse on time} - 2.32812E-004 * B. \text{Pulse off time} - 4.34333E-005 * C. \text{Servo voltage}.$$

3.3 3D Interaction graphs for MRR

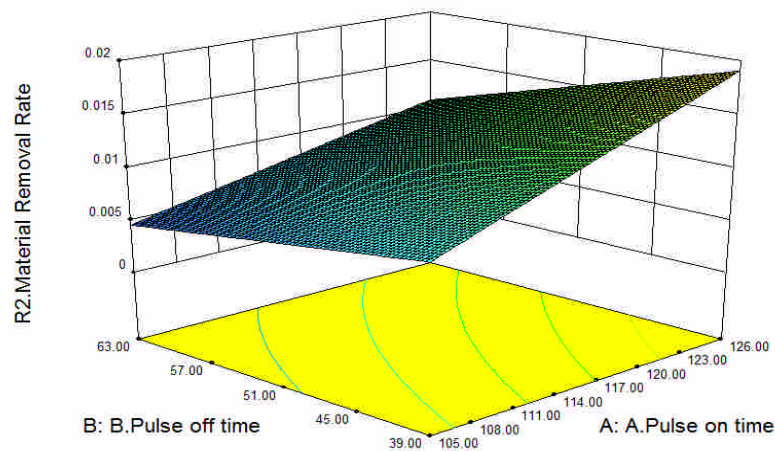


Fig 3.5 Combined Effect of Pulse on time and Pulse off time on Material Removal Rate

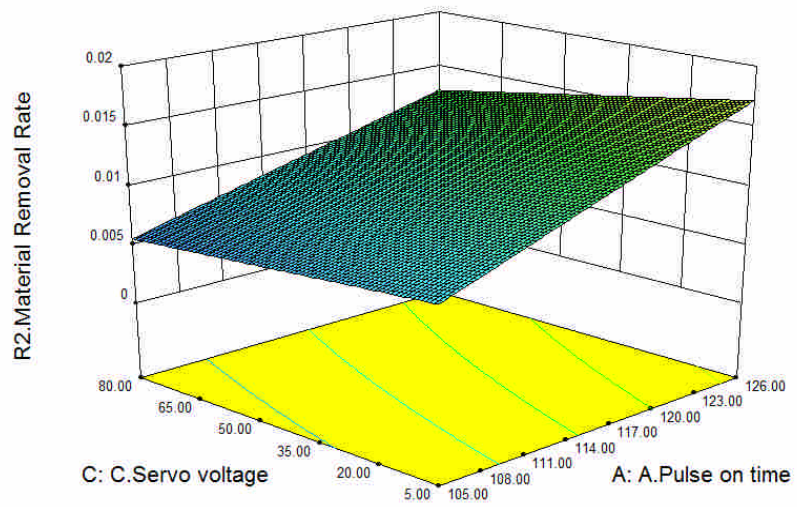


Fig 3.6 Combined Effect of Pulse on time and Servo voltage on Material Removal Rate

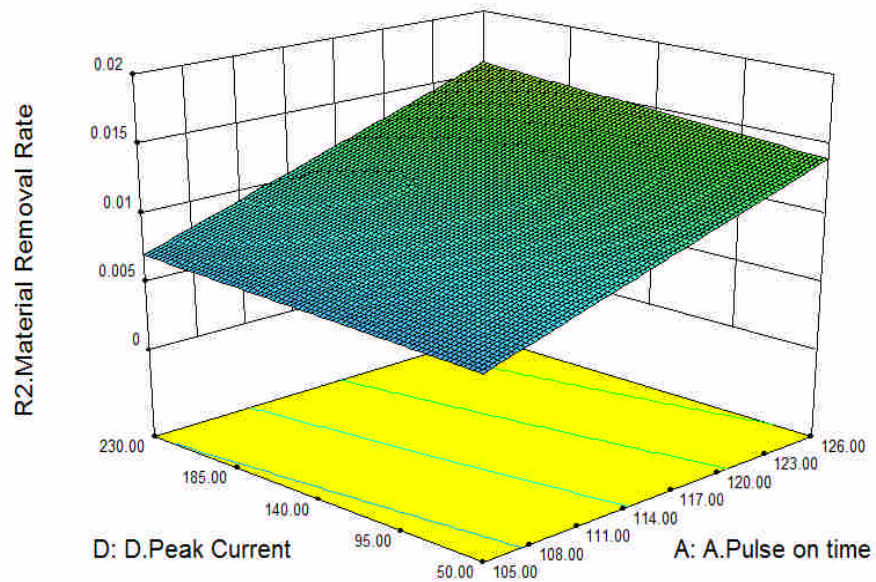


Fig 3.7 Combined Effect of Pulse on time and Peak current on Material Removal Rate

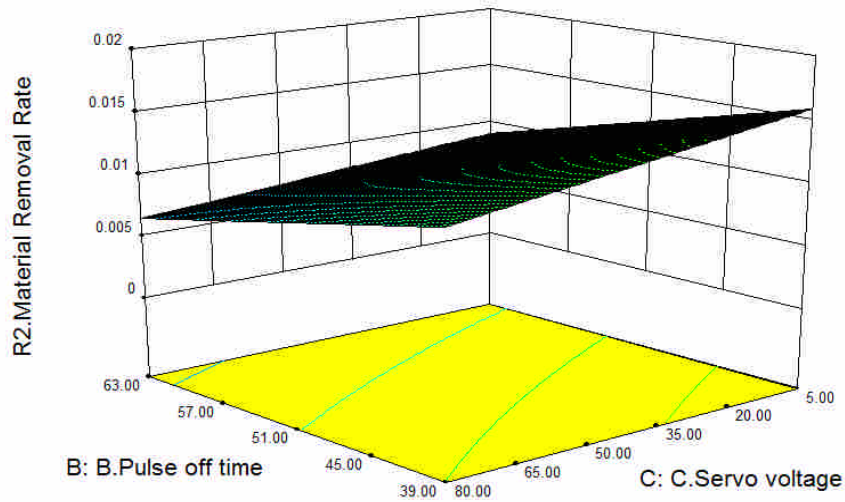


Fig 3.7 Combined Effect of Servo voltage and Pulse off time on Material Removal Rate

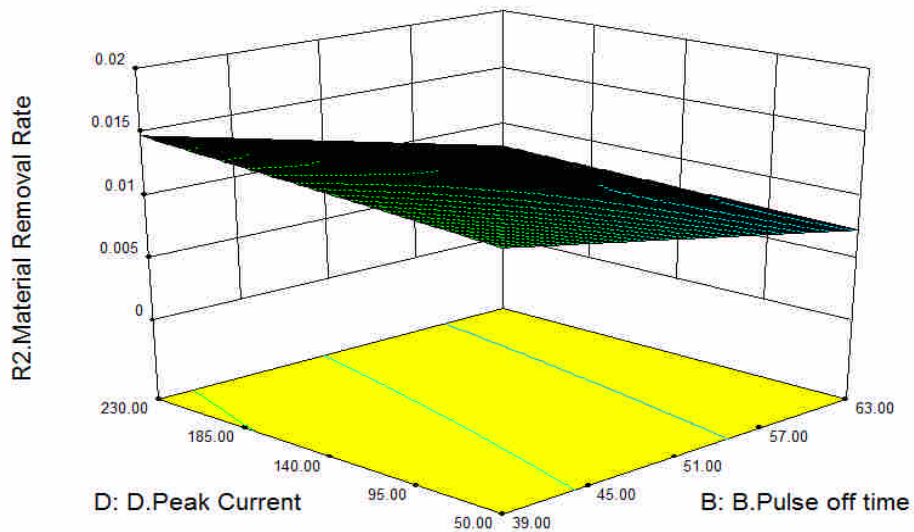


Figure 3.8 Combined Effect of Peak current and Pulse off time on Material Removal Rate

3.4 EXPERIMENTALLY CONFIRMATION TEST

Once the analyzing process for all the four responses were completed, the factors need to be optimized

according to the effects correlation and met with the objective and goal of each response. In the other words, the confirmation tests needs to be carried out in order to ensure that the theoretical predicted for optimum results using the software was accepted. All the parameters used in the confirmation tests were suggested by the Design Expert software are listed in Table 3.

Table 3: Experimentally Confirmation test results

S.No	Ton (μ s)	Toff (μ s)	SV (v)	IP (A)	Machining distance (mm)	Machining Time (min)	MRR
1	111.50	51	42.50	140	10	9.701	0.0114

CONCLUSION:

The below mentioned conclusions are derived in machining of tungsten carbide by using WEDM. The effect of various machining parameters on material removal rate are studied by adopting two level full factorial design of experiments. It is observed that when Ton value is increased from 105 μ s to 126 μ s an increment of MRR was approximately 59.41%. Meanwhile a reverse result was observed for Toff effect as graph showed that MRR decreased when Toff increased from 39 μ s to 63 μ s. The decrement of MRR was about 31.50% when Toff at 63 μ s. A reverse result was observed for SV effect as the graph showed that MRR decreased when SV increased from 5 volt to 80 volt. The decrement of MRR was about 9.082% when SV setting was at 80 volts.

REFERENCES

- [1] J. Benes, Cutting Difficult Machine Materials, 01/24/2007, ([http://www. American machinist.com /304/Issue/Article/False /44740/IssueS](http://www.Americanmachinist.com/304/Issue/Article/False/44740/IssueS) (last accessed on March 26, 2011)).
- [2] Y. Yasuo, S. Katsuhiko, An evaluation of difficulty in machining difficult-to-cut materials by using difficult-to-cut rating, Journal of the Japan Society for Precision Engineering 70(2004)407–411 In Japanese.

- [3] H. Singh*, R. Garg (january2009). "Effects of process parameters on material removal rate in WEDM" Journal of achievements in material manufacturing. Vol.32 and Issue1.page no: 70-74
- [4] P.K. Mishra 1997.Non conventional machining, fourteenth edition.Reprint 2012, Narosa publishing house, New Delhi,
p 132
- [5] K.H.Ho, S.T.Newman, S.Rahimifard, R.D.Allen, State of the art in wire electrical discharge machining (WEDM), International Journal of Machine Tools and Manufacture 44(2004) 1247-1259
- [6]M.-T. Yan and P.-H. Huang, Accuracy Improvement of Wire-EDM by Real-Time Wire Tension Control, Int. J. Mach. Tools Manuf., 2004, 44(7–8), p 807–814
- [7] Hewidy MS, El-Taweel TA, El-Safty MF. Modeling the machining parameters of wire electrical discharge machining of Inconel 601 using RSM. Journal of Materials Processing Technology 2005; 169:328–36.
- [8] Y.S. Liao, J.T. Huang, H.C. Su, A study on the machining parameters optimization of wire electrical discharge machining. Mater. Process. Technol. 71 (3) (1997) 487–493.
- [9] Lok YK, Lee TC (1997) Processing of advanced ceramics using the wire-cut EDM process. J Mater Proces Technol 63(1–3):839–843
- [10]J.P. Davim and L. Figueira, "Machinability evaluation in hard turning of cold work tool steel (D2) with ceramic tools using statistical techniques", Journal of Materials and Design, Vol. 28, pp. 1186–1191, 2007.
- [11] M. Velibor and M. Milos, "Optimization of surface roughness in turning alloy steel by using Taguchi method", Scientific Research and Essays, Vol. 6, No. 16, pp. 3474-3484, 2011.
- [12] J.S. Senthilkumar, P. Selvarani and R.M. Arunachalam, "Selection of machining parameters based on the analysis of surface roughness and flank wear in finish turning and facing of Inconel 718 using Taguchi technique", Emirates Journal for Engineering Research, Vol. 15, No. 2, pp. 7-14, 2010.
- [13] M. Kaladhar, K.V. Subbaiah, C.S. Rao and K.N. Rao, "Optimization of process parameters in turning of AISI202 austenitic stainless steel", ARPJ. of Engineering and Applied Sciences, Vol. 5, No. 9, pp. 79-87, 2010.
- [14]M.P. Groover, Fundamental of Modern Manufacturing: Materials, Processes, and Systems, 2nd ed, John Wiley & Sons, 2004

Suitability of Illumination at the Engineering Computer Laboratory in Lyceum International Maritime Academy

*Kuster Kar C. Colina, Lemuel Dimaunahan, Carissa Mae Ramirez, Angelita M. Pagcaliwagan
angiemendoza@yahoo.com*

Industrial Engineering Department, Lyceum of the Philippines University, Batangas City, Philippines

ABSTRACT

This study primarily aimed to determine the suitability of illumination inside the Engineering Computer Laboratory in Lyceum International Maritime Academy (LIMA). Survey shows that majority of the respondents answered that they are comfortable inside the computer laboratory. Majority of the respondents noticed a moderate level of illumination and there is a bright level of illumination in the computer laboratory. They have not noticed any dark level of illumination in the computer laboratory. Result shows that the illumination level inside the Engineering Computer Laboratory is suitable for the activities conducted inside the place especially for PC works.

Keywords: Illumination, Engineering, Laboratory

Introduction

The physical work environment can have a significant effect on safety and health and student satisfaction. Ergonomist and other specialist are often asked to determine whether the environmental conditions in particular settings are satisfactory. Dirty, cluttered, and poorly organized work and traffic are

common problems. Other potential concerns exposure to hazardous materials, temperature extremes, inadequate lighting, or noise levels. Addressing these issues requires knowledge of how environmental conditions impact people, assessment methods, and toolbox of solution.(Letho and Bucks, 2008)

According to Letho and Bucks, the natural and man-made environments people lived and work within vary greatly. In daily life people accommodate themselves to these environments in a variety of way. They employ heating system and wear warm clothing when the atmosphere is cold and use cooling system and wear light clothing when it is hot. They turn on the light when it is dark and shut doors against loud and undesirable noise. Man-made environment environments, such as those found within the buildings or other structures, can often be modified to keep them safe and comfortable. However, many environments pose challenges that cannot be solved by implementing environmental controls, for technical or economic reasons.

At the most basic level, the goal of the ergonomic designer is to ensure that the work environment is safe, comfortable, and conducive to the task people need to perform.

Lighting is important in the occupational environment for reason such as worker comfort and safety. Several factors influence the quality and quantity of lighting. Quality of light refers to factors such as contrast, brightness, glare, and color. Light is transmitted linearly through air. The direction of light can be changed, however, depending on the interaction with various media, and incident light will scatter or reflect from some surfaces. When light passes through different transparent media, it will bend or refract. In addition, when light passes through and exits a transparent medium, it will bend and defuse. (Lehto and Buck, 2008)

Illumination is directly related to the quantity of the light energy falling on a given area. Illumination is evaluated in the occupational environment to determine if lighting quality and quantity are appropriate for specific and general tasks.

The words people used to describe their environments reveal much about how lighting affects them. When people are unhappy with lighting conditions, the answer is often more light, but sometimes it should be better than light. There are many ways of improving lighting conditions that can be cheaper and more effective than simply investing in more light fixtures. Placement and maintenance of light sources is important, as is the number of light fixtures. Well-chosen paints and finishes on ceilings, walls, floors, and work surfaces can also play an important role, as can modification of the task to reduce visual demands.

Other information from Letho and Bucks, Artificial sources of light produce luminous energy in a variety of ways. An incandescent light bulb, for example, produces luminous energy when electricity passing through a filament heats it to high temperature, causing it to glow brightly.

The amount and quality of light falling on the inspected object is a very important job feature that strongly affects inspection performance. It is well documented in the ergonomics literature that greater illumination levels on targets improve human visual acuity. In more visually demanding tasks, greater illumination levels improve performance level.

The Engineering Computer Laboratory in Lyceum International Maritime Academy (LIMA) is primarily used as a classroom for graphic design, design programs, and research. Students also come into this room for computer help and/or for any of their needs including utilization of computers. This room is

also used for lectures and presentation of reports in some instances. The lighting in this room is filled with nine (9) fluorescent light fixtures. The fluorescent light helps illuminate the individual work room. When the room is fully occupied, the room is small and it has a very uncomfortable feeling when the room is filled. The computer laboratory is for exclusive use of engineering students only.

Lighting that is not appropriate for computer work is a major factor in visual discomforts such as eyestrain, burning or itchy eyes, headaches and blurred or double vision. (www.MedecineNet.com)

The laboratory has 48 computer units with Liquid Crystal Display (LCD) monitors. LCD's are flicker-free and radiation-free alternative to bulky and power-hungry cathode ray tube monitors. LCD displays are better known for their brightness and for their "sharp pixels" than for the fluorescent light they employ. Unfortunately, sun and light exposure can be harmful to LCD screens and prevent them from producing vivid and clear images as they should. (www.ehow.com)

.The proponents choose the suitability of illumination on the computer laboratory in LPU to determine the level of illuminance of light inside the computer laboratory and if there are experience as hazard like glare and etc.... Based on this study determines the suitability of illumination at the Engineering Computer Laboratory in LIMA regarding the physical environment of laboratory during the laboratory hours of the users who are the 2nd year General Engineering students, and 2nd year to 3rd year students of the College of Engineering in Lyceum of the Philippines University (LPU).

Determining if the existing number of fluorescent lights were enough to provide proper illumination to the laboratory, knowing if there other sources of light aside from fluorescent light and knowing if there is difference in perception of the user if the level of light is bright or dark are the factors being considered to

evaluate the suitability of illumination inside the Engineering Computer Laboratory in LIMA.

It is appropriate to evaluate the suitability of illumination at the Engineering laboratory in LIMA to make users or students aware on some features like illumination of their surrounding or workplace. It can be a guide on the university to be informed to the hazard experience of the student while there are inside an a computer laboratory.

For the teacher, it is good topic in their master's degree because of its uniqueness. And also to the manufacturing firm it can also used as reference on how they can boost the productivity and behavior of their employee.

OBJECTIVES OF THE STUDY

The primary objective of this study is to determine the suitability of illumination at the Engineering Computer Laboratory in LIMA. Specifically, it determined the profile of the respondents in terms of Year level, gender, Course and Age; to determine the engineering students' utilization of computer laboratory in LIMA in terms of Number of days per Week and Hours per Day, Laboratory Activities; to identify the problem noticed by the engineering students in computer laboratory in terms of Illumination and Feeling of discomfort; to determine the level of illumination inside the engineering computer is perceived by the engineering students and the use of lux meter; and to determine the implication of the finding of the study to the LPU's materials management office.

MATERIALS AND METHOD

Research Design

Descriptive type of research was utilized in the study. There are many factors that can contribute on the illumination level including the room index, reflectance of ceiling, walls, floor and any glass object that can reflect light, number of light bulb, diffuser that scatters light in all direction. Other factors include the colors of the room and furnishings and fixture. Type of light bulb is also a factor that affects the illumination level weather the bulbs are incandescent bulb, halogen light bulb, low-voltage light bulb or fluorescent light bulb.

Participants

The participants of this research are 82 enrolled in Computer Engineering, General Engineering and 3 Professors of Engineering Department of Lyceum of the Philippines University.

Instrument

The proponents used the lux meter to able to measure the illumination of light produce by the artificial lamp. Also they used questionnaire to be answered by the students with classes in the computer laboratory.

Data Gathering Procedure

Consideration includes the distance of light bulb from where the measurement is taken, the reflectance created by the wall, monitor, ceiling and glass board, the light from outside the room entering from the windows. The researchers also consider the answer of the respondents who are the Engineering students of Lyceum of the Philippines University in Batangas and their 3 professors through the help of questionnaire.

The researchers consult an expert called ophthalmologist and found out that the reason why perception of the respondents varied was that it is possible that they have astigmatism or color blindness but the ophthalmologist is not saying all of the respondents, just some of them. The ophthalmologist added that it is also the reason why some of the respondents said that they are experiencing eyestrain, dizziness and attention problem.

Statistical Treatment

After considering factors including age, gender, duration of usage on the laboratory, and the problems encountered by the respondents. By measuring the level of illumination inside the Engineering Computer Laboratory in LIMA, the researchers obtained the average measurement. By merging the average measurement together with the evaluated response of the respondents, it is safe to say that the illumination level inside the Engineering Computer Laboratory is suitable for the activities conducted inside the place especially for PC works.

This study utilized the following statistical tools: Frequency count, percentage, rank and weighted mean.

RESULTS AND DISCUSSION

Table 1 presents the profile of 82 respondents in terms of age, gender, course and year of the respondents from some of the students and 3 Professors of Engineering Department of Lyceum of the Philippines University.

Table 1
Frequency Distribution of Respondents According to their Profile

	Profile	Frequency	%
Year Level	2	66	80.49
	3	13	15.85
	Other	3	3.658
	Total	82	100
Gender	Male	64	78.05
	Female	18	21.95
	Total	82	100

Table 1 (CONT.)
Frequency Distribution of Respondents According to their Profile

	Profile	Frequency	%
Course	General Engineering	50	60.97
	BSCpE	29	35.37
	Other	3	3.658
	Total	82	100
Age	17	40	48.88
	18	32	39.02
	19	5	6.098
	20	2	2.44
	Above 21	3	3.66
	Total	82	100

In the year level category, there is no respondent from the 1st, 4th, 5th because they are not using the Computer Engineering Laboratory during 1st Semester SY 2012-2013. The 2nd year level is the largest having 66 or 80.49 percent, followed by 3rd year college having fourteen 13 or 15.85 percent, and three 3 professors or 3.6 percent. In the gender category, majority of the respondents were male having sixty-five

64 or 78.05 percent against female respondents having 18 or 21.69 percent.

In terms of degree program , majority of the respondents are enrolled in General Engineering having 50 or 61 percent, followed by Computer Engineering students having twenty-nine 29 or 35 percent.

Forty (40) out of 82 respondents or 48.88 percent is 17 years old, 32 students or 39.02 percent are 18 years old. Five (5) respondents or 6.098 percent are 19 years old and four (4) or 4.89 percent of the respondents are 21 years of age. Two (2) respondents or 2.44 percent are 20 years old.

Table 2
Utilization of Engineering Computer Laboratory in LIMA In Terms of Days

Number of Days	Frequency	%	<CF	>CF
1	9	10.84	82	9
2	62	75.90	73	71
3	11	13.25	11	82
Total	82	100		

Note: <CF stands for less than cumulative frequency

>CF stands for greater than cumulative frequency

Majority of the respondents are using the Engineering Computer Laboratory twice a week with the frequency of s 63 or 75.90 percent followed by the 11 or 13.25 percent of respondents using the Computer Laboratory 3 times a week. Lastly, the remaining 9 or 10.84 percent of respondents is using the Computer Laboratory once a week.

The researchers found out that the schedule of the respondents on using the computer laboratory is usually twice a week for those who are regular students. The said schedule is either Monday and Wednesday or Tuesday and Thursday. Students who utilize the Engineering Computer Laboratory for

only once a week or more than 3 times a week are irregular students.

Table 3 shows that amount of hours that the respondents used the computer laboratory in a day. The frequency distribution regarding the number of hours a student utilized the Computer Laboratory in a day.

Table 3
Utilization of Engineering Computer Laboratory in LIMA
In Terms of Hours a Day

Hours	Frequency	%	<CF	>CF
1 and 30 mins.	6	7.23	83	6
2	3	3.61	77	9
3	13	15.66	74	22
4	8	9.64	61	30
Above 4	53	63.85	53	83
Total	83	100		

Majority of the respondents were utilizing the computer laboratory more than 4 hours with the number of fifty-three (53) or 63.85 percent respondents. Next is thirteen (13) or 15.66 percent of respondents occupying the computer laboratory 3 hours in a day followed by the number of respondents occupying the computer laboratory 4 hours a day with eight (8) or 9.64 percent then six (6) or 7.23 percent of the respondent using the laboratory within 1 hour and 30 minutes. The remaining three (3) or 3.61 percent occupies the laboratory for two hours.

The largest portion of the respondents occupy the laboratory for more than four hours because they have two subject scheduled in a single day 1 with 2 hours and another with 3 hours.

Activities usually Done inside the Engineering Computer Laboratory in LIMA

Table 4 shows the different activities done by the proponent's and professor inside the computer laboratory in LPU.

Table 4
Activities Done Inside the Engineering Computer Laboratory

Activities	Frequency	%	<CF	>CF
AutoCAD	50	60.24	83	50
Programming	10	12.05	33	60
Research	5	6.02	23	65
Other: CISCO&	18	21.69	18	83
Total	83	100		

Majority of the respondents said that they usually conduct graphic designing inside the computer laboratory with the frequency of fifty (50) or 60.24 percent. 10 responses or 12.05 percent uses the laboratory for programming, five (5) responses or 6.02 percent uses it for research while eighteen (18) responses or 21.69% uses the Engineering Computer Laboratory for other purposes.

Majority of the respondents conducts graphic designing because of their subject AutoCAD while some responded other because they also conduct typing and lecture inside the computer laboratory

Table 5 shows some problems noticed inside the computer laboratory.

Table 5
Problems Noticed Inside the Engineering Computer Laboratory

Problems	Frequency	%	<CF	>CF
Insufficient light	9	10.84	83	9
Too much light	3	3.61	74	12
Improper contrast	11	13.25	71	23
Poorly distributed light	19	22.89	60	42
Flicker	7	8.43	41	49
Others	33	40.96	34	83
Total	82	100		

Majority of the responses indicate other problems but what they indicate is not related about the research while other who answered none indicated that they noticed any problem with the frequency of thirty-four (34) or 40.96 percent followed by poorly distributed light inside the computer laboratory with nineteen (19) or 22.89 percent respondents after that is eleven (11) or 13.25 percent of respondents who answered improper contrast. Then some respondents answered that they noticed insufficient light with the frequency of nine (9) or 10.84 percent. Seven (7) or 8.43 percent of respondents answered flicker. Lastly, three (3) or 3.61 percent respondents answered that they noticed too much light.

The researchers found out that skylights and windows should be located and spaced so that daylight conditions are fairly uniform over the working area. Where necessary, skylights and windows should be provided with means to avoid glare. Artificial lighting shall be provided when daylight fails or for area where the daylight illumination is insufficient. The general lighting should be of uniform level, widely distributed to avoid harsh shadows or strong contrast and free from direct or reflected glare. Where intense local lighting is necessary, a combination of general and supplementary lighting at the point of work may be provided. Supplementary lighting shall be specially designed for the particular visual task and arranged or provided with shading or diffusing devices to prevent glare.

Table 6 shows the number of the respondents if they feel discomfort inside the engineering laboratory.

Table 6
Feeling of Discomfort inside the Engineering Computer Laboratory

Choices	Frequency	%	<CF	>CF
Yes	30	37.35	83	31
No	52	62.65	52	83
Total	82	100		

Majority of the respondents answered no, they don't feel any discomfort inside the computer laboratory with the frequency of fifty-two (52) or 62.65 percent and the remaining respondents answered yes with the number of thirty-one (31) or 37.35 percent

Table 7 shows the percentage of discomfort inside the Engineering Computer laboratory.

Table 7
Discomfort inside the Engineering Computer Laboratory

Problems	Frequency	%	<CF	>CF
Glare	0	0	31	0
Eyestrain	17	54.84	31	17
Anxiety	0	0	14	17
Hyper Activity	6	19.36	14	23
Attention Problem	3	9.68	8	26
Others: Headache	5	16.13	5	31
Total	31	100		

Majority of the respondents are experiencing eyestrain with the frequency of seventeen (17) or 54.84 percent. Followed by 19.36 percent respondents who answered feeling of hyper activity; five (5) or

16.13 percent of the respondents answered other and they indicate that they experienced dizziness. Then the remaining three (3) or 9.68 percent of respondents answered that they experienced attention problem while there is no one answered of feeling of glare and anxiety.

It is said from the related literature that lighting that is not appropriate for computer work is a major factor in visual discomforts such as eyestrain, burning or itchy eyes, headaches and blurred or double vision. Lighting should be adequate for you to see the text and the screen, but not so bright as to cause glare or discomfort. Artificial lighting shall be adequate at the place of work for the operation or work performed. Poor lighting can cause several problems such as: insufficient light - not enough light for the need, glare - too much light for the need, improper contrast, poorly distributed light, and flicker. Things know about insufficient light poor lighting can be a safety hazard - misjudgment of the position, shape or speed of an object can lead to accidents and injury. Poor lighting can affect the quality of work, specifically in situation where precision is required, and overall productivity. Poor lighting can be a health hazard - too much or too little light strains eyes and may cause eye discomfort and headaches. Research in the use of light in schools has shown that cool-white fluorescent bulbs cause: bodily stress, anxiety, hyper-activity, attention problems and other distress leading to poor learning performance.

Table 8 shows the level of illumination inside the Engineering Computer Laboratory based on moderate and bright.

Table 8
Level of Illumination inside the Engineering Computer Laboratory

Level	Frequeuncv	%	<CF	>CF
Moderate	70	84.34	12	70

Bright	12	15.66	82	82
Total	82	100		

Majority of the respondents noticed a moderate level of illumination with the frequency of seventy (70) or 84.34 percent. The next level of illumination noticed by the respondents is the bright level of illumination with thirteen (13) frequencies or 15.66 percent. The last level of illumination is the dark level of illumination with the frequency of zero (0) or 0 percent, this means that no one noticed or answer a dark illumination in the computer laboratory.

According on the book written by Lehto and Buck, lighting can have negative effect on performance, morale, and safety. Part of the issue is that poor lighting can interfere directly with the task people perform because vision is one of the major senses guiding human activities. Hence, inadequate lighting can cause people to misread signs or instruments, or make other mistakes, resulting in lower productivity and reduce safety. Poor lighting also has a major impact on people's subjective reactions to their environment. Bright light on the display screen "washes out" images making it difficult for operators to clearly see the work.

According on the book written by Lehto and Buck, lighting can have negative effect on performance, morale, and safety. Part of the issue is that poor lighting can interfere directly with the task people perform because vision is one of the major senses guiding human activities. Hence, inadequate lighting can cause people to misread signs or instruments, or make other mistakes, resulting in lower productivity and reduce safety. Poor lighting also has a major impact on people's subjective reactions to

their environment. Bright light on the display screen "washes out" images making it difficult for operators to clearly see the work.

Table 9 shows the level of illumination produce of different florescent lamp inside the computer laboratory in LPU based on different location.

Table 9
Level of Illumination inside the Computer Laboratory

No. of Lamps	Illumination on North direction	Illumination on East direction	Illumination on West direction	Illumination on South direction
1	84.0	75.6	84.1	77.1
2	83.9	84.1	57.5	77.7
3	57.2	57.5	57.6	54.3
4	77.1	57.5	76.7	73.2
5	77.7	76.7	64.5	74.5
6	54.3	64.5	55.6	62.7
7	73.2	81.2	67.6	62.6
		67.6	56.1	62.7
8	62.7			
9	62.7	56.1	59.6	64.1

Note: All units are in LUX

Table 10 shows the max illuminance produce by different florescent lamp installed inside the computer laboratory.

Table 10
Level of Illumination Produce by the Florescent Lamp

No. of Lamps	Illumination Level
1	561
2	620
3	583
4	503
5	585
6	547
7	688

8	506
9	568
Total	573.44

Note: All units are in LUX

The level of illumination from the light bulbs varies because of the age of the bulbs or the duration from the period when the bulb was installed in the Engineering Computer Laboratory up to the period when measuring the level of illumination was conducted. The average illumination level produced by the light bulbs is 573.44 lux which is in the range of 500-1000 lux for Normal Office Work, Study Library, Groceries, Show Rooms, and Laboratories especially for PC works.

The illumination level inside the Engineering Computer Laboratory in LIMA is 67.93 which is the range of 51-100 lux for working spaces where visual tasks are only occasionally performed.

CONCLUSION

There are many considerations involved on determining the illumination in the computer laboratory. Based on the proponents observation that color absorb the light produced by the florescent lamp, and the placement of the florescent are arrange to able to light the area. By getting the measurement of illumination emitted by the light bulbs and the illumination level in certain areas in the computer laboratory using a Lux Meter, the researchers come up with the average illumination level which fell inside the recommended level of illumination for Laboratory and PC works. It means the level of illumination inside the Engineering Computer Laboratory is suitable for activities especially for PC works. The proponents measure illuminance on morning which there is no classes on the computer laboratory

using the lux meter.

The following statements are potential hazards in some certain computer laboratory that can be related to the problems of Engineering Computer Laboratory in LIMA: bright light on the display screen "washes out" images making it difficult for operators to clearly see the work; bright light in the operator's field of view; and high contrast between light and dark areas of the computer screen, horizontal work surface, and surrounding areas.

RECOMMENDATION

In case of improper illumination level, for example is flicker of fluorescent light, replacement is required for optimum performance. Use light diffusers so that desk tasks can be performed without direct brightness on the computer screen. Place rows of lights parallel to the operator's line of sight. Use operator adjustable task/desk lighting. If diffusers or alternative lights are not available, removing the middle bulbs of 4-bulb fluorescent light fixtures can also reduce the brightness of the light. Use blinds or drapes on windows to eliminate bright light. Blinds should be adjusted during the day to allow light into the room, but not directly into the operator's field of view. Lamps should have glare shields or shades and the line of sight from the eye to the light should be at an angle greater than 30 degrees. Reorient the work-station so that bright lights from open windows are not in the field of view. Use indirect or shielded lighting where possible and avoid intense or uneven lighting in the field of vision.

For computer work, well-distributed diffuse light is best. The advantages of diffuse lighting are

two-fold: There tend to be fewer hot spots, or glare surfaces, in the visual field, and the contrasts created by the shape of objects tend to be softer.

Students utilizing the computer laboratory should take great care to avoid eye strain which leads to safety threats. In case of any eye problem, immediately approach the faculty member assigned to their class.

Future researchers may dealt with the suitability of illumination inside the other computer laboratories and offices of LPU

REFERENCES

- Illumination, url: <http://www.MedicineNet.com/illumination>, June 29, 2012
- Kroemer, Karl, Henrike Kroemer and Katrin Kroemer- Elbert,: 2001 Ergonomics: How to Design For Ease and Efficiency Upper Saddle River, NJ., c2001.xx, 695p:ill,:25cm Second Edition
- Letho, Mark and James R. Buck, (year): Introduction To Human Factors and Ergonomics for Engineering
Lightning
evaluation, url: <http://amberharreliar431.blogspot.com/2009/02/lighting-evaluation-of-iarccomputer.html>, June 29, 2012
- LightingforSchool, url: http://www.fullspectrumsolution.com/lighting_for_school.stml, June 29, 2012
- Sanders, Mark S. and Mc Cornick, Ernest J., (n.d.): Human Factors and Ergonomics for Engineering

Analysis for controlling belt deviation in conveyor system

Ankit Gupta

Department of Mechanical Engineering, MITS College Gwalior (M.P.) India

Email: aankitgupta89@gmail.com

ABSTRACT: In this paper an analysis of maintenance data of the two different structural components used for controlling belt deviation in conveyor system, working in coal handling plant of thermal power plant has been done. The new set-up of controlling belt deviation has been compared with the present set-up on the maintenance ground to find out the effectiveness of the new hydraulic control system. The new set-up consists of hydraulic control self aligning idlers with displacement sensor, is compared with the present set-up of mechanically controlled self aligning idler system.

Keywords: belt, conveyor system, failure, self-aligning-idler, hydraulic control

INTRODUCTION

Belt conveyors are, in most cases, the most cost-effective solution for bulk material handling for shorter and medium distance. The belt is the key component of these conveyors because its cost is approx. 25 ~ 50% of the total cost. As per the maintenance data of the coal handling system working in the thermal power plant, the root cause founded for all the failure in the belt is deviation of belt, so there is a need to develop an advance system for controlling it. Tracking or training is the procedure required to make the conveyor belt run true when empty or fully loaded. It is the process of adjusting idlers to correct any tendencies of the belt to run other than true.

[1] Lihua Zhao has worked for the failure analysis and processing of belt conveyor system, [2] Lihua Zhao has done the work on the operation and maintenance of conveyor system in thermal power plant, the main issues of the system maintenance and failure derived by the research of Lihua Zhao was that of belt deviation. [3] Lihua Zhao has worked for the adjustment method of conveyor belt deviation, adding to that this research has been made. [4] Zhang Jia-wei, Lou Pei-huang has provided the method for automatically detection of the belt deviation and controlling it hydraulically so that the adjustment of the belt can run on the true position.

The research department has installed hydraulic control system with displacement sensor in one of the conveyor system running parallel to the present system having self aligning idler installed with it for

controlling belt deviation. The comparative maintenance data of both the system working in same condition proved that hydraulic control system is much more effective in controlling belt deviation and hence it must be used in other conveyor system for reducing failure due to deviation.

PRESENT SET-UP

Present set up consists of self aligning idlers. The arrangement of self-aligning-idler is installed at the carrying side and return side at an interval of 15m on the carrying run and 30m at the return run.

Fig.1 shows the set of self aligning idler or the training idler that works for the controlling of belt deviation mechanically. It is mounted with the idlers on both the sides of the conveyor i.e. at the carrying side and at the return side also. It consists of an ordinary troughed three roller idler (1), mounted on swivel frame (2), which is free to swivel within a limit about a vertical pivot (3). When the belt shifts off the centre, the edge contracts on actuating roller (4) with a slight pressure, and makes the idler take a skewed position when a force acts which tends to steer the belt back to its central position. As the belt return to its central position, it automatically returns the idler to its initial position.

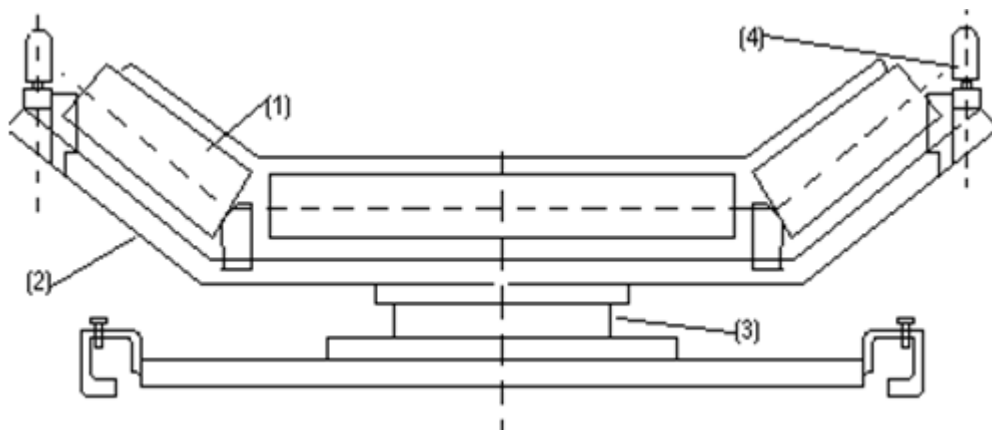


Fig.1. Centering idler or self-aligning-idler



Fig.2. Image of Centering idler or self-aligning-idler

EXPERIMENTAL SET-UP

This set-up consists of hydraulic control self-aligning idler with displacement sensor. Here the set up is similar to the centering idler but the efficiency and sensing capability increases with the use of hydraulic displacement sensor. This sensor detects the deviation of belt and provides the similar action of controlling the deviation as in self aligning idlers but with greater efficiency. The sensor controls the deviation of belt within its fixed range but when the situation come that it is out of the sensor range it provide emergency stop to the system and induce an alarm so that the place of the fault can be easily detected and can be repaired with no time lose and prevent the damage of the belt.

Fig.3 shows the set of self aligning idler or the training idler that works for the controlling of belt deviation hydraulically. It is mounted with the idlers on both the sides of the conveyor i.e. at the carrying side and at the return side also, which consists of an ordinary troughed three roller idler, mounted on swivel frame (2), which is free to swivel within a limit about a vertical pivot (3). When the belt shifts off the centre, the edge contracts displacement sensor (1) which acts as a switch and allows the hydraulic fluid to pass through from the tube (4) and reaches fuel sump (3) from where it passes to main cylinder, with a slight pressure makes the idler to take a skewed position when a force acts which tends to steer the belt back to its central position. As the belt return to its central position, it automatically returns the idler to its initial position.

But in case the deviation of belt is much higher than the range of the displacement sensor i.e. when the cylinder elongation is at maximum position the sensor puts the conveyor on emergency stop and sets the alarm on. So that fault position can be located easily and can be rectified on time.

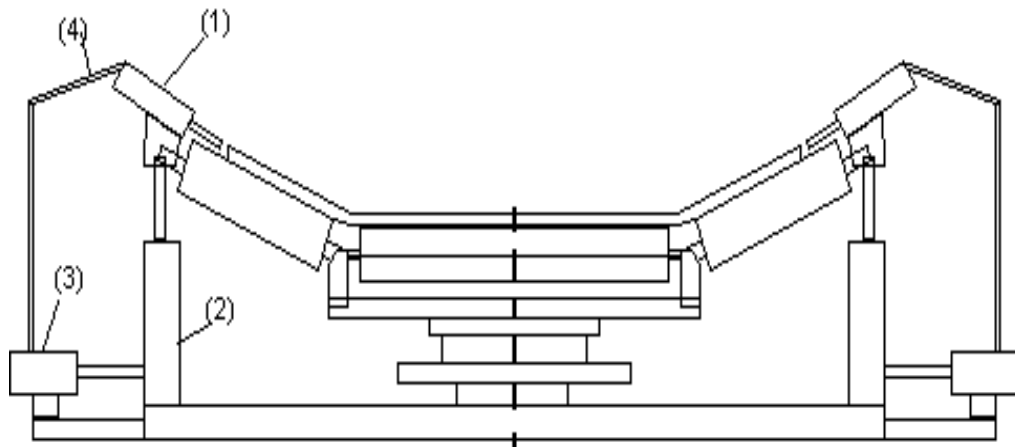


Fig.3. Hydraulic control self-aligning-idler with displacement sensor



Fig.4. Image of Hydraulic control self-aligning-idler with displacement sensor

COMPARISON OF MAINTENANCE DATA ON SET-UP

The data are taken from the thermal power plant where the system is set-up for recording the no. of working hour wasted in maintenance of the conveyor. The data are drawn under same working condition, under similar condition of belt and idlers.

Table1: Maintenance Data sheet of 6 month

S.No.	Maintenance management	No. of maintenance work on Hydraulic control self-aligning-idler	No. of maintenance work on self-aligning-idler	Time for maintenance on Hydraulic control self-aligning-idler	Time for maintenance on self-aligning-idler
1	Breakdown maintenance (due to deviation)	1	4	3 hr	12hr
2	Breakdown maintenance (other breakdown)	1	2	2hr	3hr
3	Preventive maintenance	5	3	7hr	3hr
4	Scheduled maintenance	6	6	15hr	12hr
	Total	13	15	27hr	30hr

RESULT

The data sheet clearly shows that the no. of break down due to deviation that occurred in the mechanically controlled self aligning is much more then hydraulic control self-aligning-idler; hence the data shows that the advance system of controlling the belt deviation is much effective in controlling the belt deviation. The working hour wastage due to maintenance work on the advance hydraulic control self-aligning-idler is less than the time wasted on the mechanically control self-aligning-idler.

CONCLUSION

Based on the analysis of maintenance data of the two different structural components used for controlling belt deviation in conveyor system, working in coal handling plant of thermal power plant, it is clear that the new set-up of controlling belt deviation, compared with the present set-up on the maintenance ground is found out much effective. The maintenance data sheet clearly suggests that the maintenance work can be reduced up by using Hydraulic control self-aligning-idler and it also reduces the breakdown of belt due

to deviation.

ACKNOWLEDGMENT

The Authors express his gratitude to the management of Parichha thermal power plant, Jhansi and to the faculty of MITS for their valuable support and help in my work.

REFERENCES

- [1] Lihua Zhao. “Typical failure analysis and processing of belt conveyor”, [J]. Hoisting and Conveying Machinery; 2003, No. 10.
- [2] Lihua Zhao, Yin Lin. “Operation and Maintenance of Coal Handling System in Thermal Power Plant”, [J]. Colliery Machine; 2011, No. 02.
- [3] Lihua Zhao. “The adjustment method of conveyor belt deviation”, [J]. Colliery Machine; 2001, No. 10.
- [4] Zhang Jia-wei, Lou Pei-huang, “Automatic detection and hydraulic correction technology of belt deviation” mechanical engineer, 2008- en.cnki.com
- [5] Raghvendra Singh Gurjar, “Failure analysis of belt conveyor system”, [J]. IJESS Volume 2, Issue 10, 2012
- [6] Marianna Tomašková, Daniela Marasová, “Analysis of the operational risks of a belt conveyor using the method of determining the object limits”. No. 4, Volume VII, December 2012
- [7] Yusong Pang, Gabriel Lodewijks, “Large-scale Conveyor Belt System Maintenance Decision-making by Using Fuzzy Causal Modeling”, Proceedings of the 8th International IEEE Conference on Intelligent Transportation Systems Vienna, Austria, September 13-16, 2005

Determination of Delamination and Surface Roughness for Machined Fiber Reinforced Plastics using Machine Vision

G Dilli Babu^{1,*}, K. Sivaji Babu², B. Uma Maheswar Gowd³

¹Mechanical Engineering Department, V R Siddhartha Engineering College, Vijayawada-520 007, India

²Mechanical Engineering Department, P.V.P. Siddhartha Institute of Technology, Vijayawada-520007, India

³ Mechanical Engineering Department, J. N. T. U. college of Engineering, Anantapur-515002, India

Email: *gdillibabu@gmail.com , Phone: 00919393271212, Fax: 0091 866 2582672 (Corresponding author)

Abstract

The inspection of delamination and surface roughness of the machined Fiber Reinforced Plastics is very important to assess the quality of a composite, which is normally carried out using Tool maker's microscope and taly-surf devices, respectively. This method of measuring is accepted widely by all the researchers. But, this process is not suitable for high volume applications as it is time consuming and cumbersome. With rising demand of industrial automation in manufacturing process, machine vision technique plays an important role in inspection and process monitoring. In this paper, new parameters for determining delamination and surface roughness of machined fiber reinforced specimens were proposed using machine vision technique. The experimental result indicates that the delaminations and surface roughness of machined composites could be predicted with a reasonable accuracy using machine vision.

Keywords: Delamination, Surface Roughness, Machine Vision.

1. Introduction:

Most of the composite products are made to a near-net shape, a certain degree of intricacy in the product design necessitates the development of the composite product in parts. The independently manufactured parts are then finally assembled to get the final composite product. Machining thus becomes imperative to ascertain the structural integrity of complex composite products. Though a number of approaches have been used for machining composite laminates, conventional drilling and milling till date is the most widely acceptable and frequently practiced machining operation. Conventional drilling and milling however results in damage in the form of delamination, micro cracks, surface roughness and matrix burning and may ultimately cause variation in the strength of the component. [1-5].

Miller [6] presented in 1987 a database on optimum cutting parameters for drilling holes with minimum local machining damage. Lin et al. [7] in 1996, carried out a study on drilling of carbon fiber reinforced composite at high speed and concluded that an increase of the cutting velocity leads a increasing of the drill wear. In this way the fact of increasing the wear of drill causes a rising of thrust force. Piquet et al. [8] in 2000 carried out a study of drilling thin carbon/epoxy laminates with two types

of drills, a helical drill and a drill of special geometry, and concluded that both drills leads a damage at the entrance in the wall and the exit of the hole, with the exception of special geometry drill which is possible a significant reduction in the final damage. Enemuoh et al. [9] in 2001, realize that with the application of the technique of Taguchi and other methods, were possible to achieve the cutting parameters that allowed the absence of damage in the drilling of fiber reinforced plastics.

In the above literature the delamination was measured using tool maker's microscope and surface roughness was measured using stylus instrument. But these methods are not suitable for automating the measurement process.

Specifically, high-speed measurement of delamination and surface roughness is desired, which is possible using optical means. The techniques for delamination and surface roughness measurements must be applicable for shop-floor implementation. Machine vision is proposed in this work as an attractive and yet inexpensive option for online delamination and surface roughness measurements. Machine vision has been very successfully employed in several manufacturing applications including material handling, assembly and inspection [10]. Some attempts were made to measure surface roughness using machine vision also. Most of the methods are based on statistical analysis of grey-level images in the spatial domain.

M. Kiran at al. [11] proposed roughness related value could be estimated by computing the variance of the intensity distribution of the different surface images under a fixed illumination set up. For medium rough surfaces the correlation was good. And also a second order statistic to describe the surface texture "texture unit" which describes the local texture aspect of a given pixel was proposed. Du-Ming Tsai at al. [12] proposed a machine vision system for the classification of castings. The method of assessing surface quality is based on the two-dimensional Fourier Transform of a cast surface in both gray level image and binary image. The Bays classifier and neural network classifier are implemented for roughness classification. M. Gupta at al. [13] tried to characterize the surface roughness by calculating the intensity of the light reflected from the machined surface. They conducted experiments both on stationary and rotating surfaces and proposed two parameters. They calculated standard deviation, mean, root mean square (RMS) of the gray level intensity distribution. The proposed parameters R1 and R2 are calculated by dividing standard deviation with RMS and standard deviation with arithmetic mean respectively. And they tested the sensitivity of these parameters to the differences in surface roughness, ambient light and spindle speed and shown that these vision parameters can discriminate the different surface roughness heights and insensitive to ambient lighting and speed rotation. S.Y. Ho at al. [14] proposed another method by using an adaptive neuro-fuzzy inference system to predict the roughness of the turned surfaces better.

In this work, the feasibility of using an inexpensive vision system for the optical characterization of machined natural fiber reinforced composite surfaces was studied. New parameters for determining delamination and surface roughness of machined fiber reinforced specimens were proposed using machine vision technique.

2. Plan of Experiment:

Delamination and surface roughness of machined fiber reinforced composites depends on many factors like machining parameters (cutting speed, feed rate etc), cutting tool properties, work piece properties, machine tool vibrations etc. Here, for this experimental purpose the predominant factors which affect the delamination and surface finish (cutting speed, and feed rate) were considered. Remaining all other controllable factors was kept constant. The composite materials used in the experiments are made with different fiber reinforcements, such as Banana Fiber Reinforced Plastics (BFRP), Jute Fiber Reinforced Plastics (JFRP), Hemp Fiber Reinforced Plastics (HFRP), Vakka Fiber Reinforced Plastics (VFRP) and Glass Fiber Reinforced Plastics (GFRP). The polyester resin possessing a modulus of 3.25 GPa and density 1350 kg/m³ was used in preparing the specimens.

Table 1 indicates the two machining parameters (cutting speed and feed rate) to be studied and the assignment of the corresponding levels (low, center, high). A L₉ orthogonal array is selected for the present investigation, which has 9 rows corresponding to the number of tests (eight degrees of freedom) with two columns at three levels, as shown in Table 2. The plan of experiments is made of nine tests (array rows) in which the first column was assigned to the cutting velocity and the second column to the feed rate and the remaining were assigned to the interactions. The machining process responses to be studied are delamination, and surface roughness in various fiber reinforced plastic (FRP) composites.

The sequential steps followed during the experiments were as follows. First, surfaces of different delamination values and surface roughness values were created using CNC milling centre and images of those work pieces are taken using a Nikon cool pix L22 digital camera under proper illumination conditions. Those images were analyzed using package Mat Lab 7.0. The results are compared with Tool maker's microscope and taly-surf device parameters.

Table 1. Levels of the variables used in the experiment.

Process parameters	Low (1)	Center (2)	High (3)
Cutting speed in m/min	16	24	32
Feed rate in mm/rev	0.10	0.20	0.30

Table 2. Orthogonal array L₉ (2⁴) of Taguchi design.

L ₉ (2 ⁴) Test	1	2	3	4
1	1	1	1	1
2	1	2	2	2
3	1	3	3	3
4	2	1	2	3
5	2	2	3	1
6	2	3	1	2
7	3	1	3	2
8	3	2	1	3
9	3	3	2	1

3. Vision-Based Parameters Computed

3.1. Delamination area (D_a) for delamination measurement

This method is based on the block and white image of the machined fiber reinforced plastic composites (Figure 1). A parameter called Delamination area (D_a) is proposed for determining machined delaminations of different fiber reinforced composites. Delamination area (D_a) estimates the area of all the on pixels in an image by summing the areas of each pixel in the image. Total is a scalar whose value corresponds roughly to the total number of on pixels in the binary image, but might not be exactly the same because different patterns of image pixels are weighted differently. The image area of an individual pixel is determined by looking at its 2-by-2 neighborhood. There are six different image pixel patterns, each representing a different area value:

- Image pixel patterns with zero on pixels (area = 0)
- Image pixel patterns with one on pixel (area = 1/4)
- Image pixel patterns with two adjacent on pixels (area = 1/2)
- Image pixel patterns with two diagonal on pixels (area = 3/4)
- Image pixel patterns with three on pixels (area = 7/8)
- Image pixel patterns with all four on pixels (area = 1)

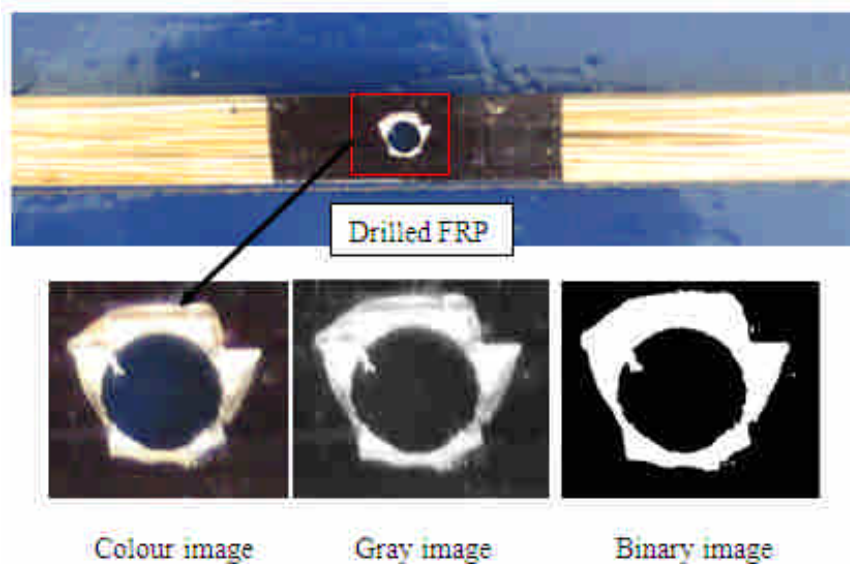


Fig. 1. Digital image processing for determining delamination area (D_a).

3.2. Co-efficient of Variance (CV) for surface roughness (R_a) measurement:

The co-efficient of variance (CV) method is based on the relative gray level intensity of the each pixel with its surrounding pixels (Figure. 2). It is assumed that the peaks on any surface will reflect more light than its surrounding surfaces and statistical parameter is calculated based on the distribution of these

peaks. Here the gray image is converted into binary image by assigning “1s” for image pixel having more intensity values than its surrounding pixels in the 3X3 cell and remaining all into “0s”. Mean and standard deviation of the binary images were determined. The co-efficient of variance of the binary image was computed using:

$$\text{Co-efficient of variance} = \left(\frac{\text{Standard deviation of binary image}}{\text{Mean intensity values of binary image}} \right) \times 100$$

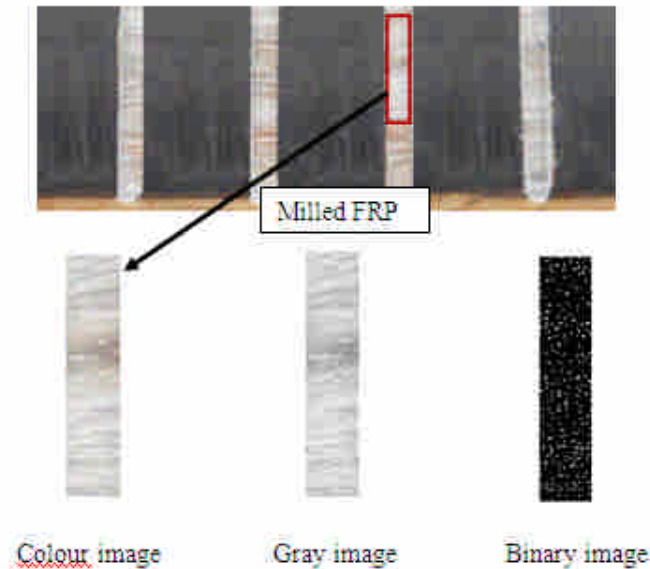


Fig. 2. Digital image processing for determining Co-efficient of variance (CV).

4. Results and Discussion of Delamination area (D_a)

The delamination of machined FRP specimens were calculated by using both conventional and Machine Vision based techniques. In conventional method, the delamination is determined using ‘Mitutoyo TM 500’ tool maker’s microscope [15]. It is represented as delamination factor (F_d). Table 3 presents the experimental layout plan and the computed average values of delamination factor (F_d) and proposed vision parameter delamination area (D_a) of different fiber reinforced composites.

Table 3. Experimental results of delamination factor (F_d) and delamination area (D_a).

Test	Delamination factor (F_d)					Delamination area (D_a)				
	BFRP	JFRP	HFRP	VFRP	GFRP	BFRP	JFRP	HFRP	VFRP	GFRP
1	1.46	1.70	1.70	1.94	1.56	20181	23561	25478	25147	22028
2	2.02	2.40	2.30	2.04	1.98	27065	31287	30258	30215	26749
3	2.52	3.00	2.60	2.40	2.36	35483	40218	32589	33456	37822
4	1.25	1.30	1.07	1.48	1.22	15648	18547	10985	20147	17786
5	1.61	1.35	1.30	1.68	1.64	23544	29784	21985	28167	22454
6	1.87	2.25	2.00	1.76	1.83	25894	33657	28145	28879	27606
7	1.11	1.13	1.03	1.19	1.10	12293	12657	10120	15678	11398

8	1.16	1.235	1.085	1.24	1.19	18705	26471	21078	15874	24397
9	1.38	1.55	1.42	1.56	1.52	21485	29871	24165	18712	25300

From table 3, it can be observed that the machine vision parameter value increases with an increase in delamination. This is because the amount of white scattering increases with an increase in delamination damage.

4.1. Correlation (delamination factor /delamination area):

The correlations between delamination factor (F_d) and the delamination area (D_a) in different fiber reinforced composite laminates of drilled specimens were obtained by linear regression using Minitab 16 software. The linear regression equations and correlation coefficient R^2 values are as follows,

Banana Fiber Reinforced Plastics (BFRP):

$$F_d = 0.5075 + 0.000068 D_a \quad R^2 = 95.0\% \quad (1)$$

Jute Fiber Reinforced Plastics (JFRP):

$$F_d = 0.2215 + 0.000080 D_a \quad R^2 = 95.2\% \quad (2)$$

Hemp Fiber Reinforced Plastics (HFRP):

$$F_d = 0.3236 + 0.000067 D_a \quad R^2 = 85.6\% \quad (3)$$

Vakka Fiber Reinforced Plastics (VFRP):

$$F_d = 0.5463 + 0.000047 C2 \quad R^2 = 88.9\% \quad (4)$$

Glass Fiber Reinforced Plastics (GFRP):

$$F_d = 0.5394 + 0.000060 b\text{warea} \quad R^2 = 93.4\% \quad (5)$$

In all the selected materials, a quite good correlation between tool makers microscop parameter and vision parameter has been obtained.

5. Results and Discussion of Surface roughness (R_a) of machined composites:

The surface roughness of machined FRP specimens were calculated by using both conventional and Machine Vision based techniques. In conventional method, the average surface roughness (R_a) is determined using ‘Taly-surf’ stylus instrument [16]. Table 4 presents the experimental layout plan and the computed average values of surface roughness (R_a) and proposed vision parameter co-efficient of variance (CV) of different fiber reinforced composites.

Table 4. Experimental results of Surface roughness and Co-efficient of variance.

Test	Surface roughness (R_a)					Co-efficient of variance (CV)				
	BFRP	JFRP	HFRP	VFRP	GFRP	BFRP	JFRP	HFRP	VFRP	GFRP
1	1.870	2.352	1.405	1.237	1.610	538.5	540.2	543.2	481.0	499.2
2	2.340	2.772	1.617	2.360	2.035	563.2	541.0	559.7	500.0	501.7

3	2.945	3.885	2.792	3.352	2.617	588.5	548.5	588.5	546.5	511.7
4	1.340	1.845	1.120	0.922	1.385	541.7	534.2	541.7	480.0	499.7
5	1.952	2.742	1.347	1.722	1.872	544.5	539.2	544.5	498.0	500.7
6	2.302	3.310	2.015	2.235	1.935	560.7	543.5	560.7	508.0	507.0
7	0.932	1.755	0.907	0.955	0.845	526.0	531.2	526.0	478.0	494.2
8	1.772	2.195	1.190	1.470	1.520	533.0	532.2	533.0	489.7	497.5
9	1.922	2.465	1.830	1.920	1.840	553.0	542.2	553.0	496.5	501.5

From table 4, it can be observed that the machine vision parameter value increases with an increase in roughness. This is because the amount of diffuse light scattering increases with an increase in roughness.

5.1. Correlation (surface roughness/Co-efficient of variance) for vision results:

The correlations between the surface roughness (R_a) and the Co-efficient of variance (CV) in different fiber reinforced composite laminates of milled specimens were obtained by linear regression using Minitab 16 software. The equations obtained were as follow:

Banana Fiber Reinforced Plastics (BFRP):

$$R_a = - 13.46 + 0.02799 CV \quad R^2 = 83.2\% \quad (6)$$

Jute Fiber Reinforced Plastics (JFRP):

$$R_a = - 56.52 + 0.1096 CV \quad R^2 = 82.0\% \quad (7)$$

Hemp Fiber Reinforced Plastics (HFRP):

$$R_a = - 14.96 + 0.03006 CV \quad R^2 = 93.4\% \quad (8)$$

Vakka Fiber Reinforced Plastics (VFRP):

$$R_a = - 15.86 + 0.03549 CV \quad R^2 = 92.0\% \quad (9)$$

Glass Fiber Reinforced Plastics (GFRP):

$$R_a = - 41.48 + 0.08618 CV \quad R^2 = 82.5\% \quad (10)$$

In all the selected materials, a quite good correlation between stylus parameter and vision parameter has been obtained.

6. Conclusions

From the results of the proposed machine vision parameters for delamination and average surface roughness of the machined natural fiber reinforced composites, the following can be concluded from the present study within the range of the experiments.

- (1) The feasibility of using an inexpensive vision system for the optical characterization of machined delaminations and surface roughness was demonstrated.
- (2) Parameters derived from the image of the optical scatter spectrum were investigated for differentiating between surfaces of different delamination and roughness values.

- (3) Two new machine vision parameters were introduced for determining the delaminations and surface roughness of the fiber reinforced composites.
- (4) It was found that the delamination and roughness of the surfaces conclusively affects the vision parameters.
- (5) The machine vision parameters are having good correlation with microscope measured delamination factor (F_d) and stylus measured average roughness (R_a).
- (6) From the regression equation it is clear that the machine vision parameters are depending on the colour of the material, so separate regression equation is necessary for each coloured materials.

References

1. K. Palanikumara, J. Paulo Davim. Assessment of some factors influencing tool wear on the machining of glass fibre-reinforced plastics by coated cemented carbide tools. *Journal of materials processing technology*. 209, 2009, 511–519.
2. N. Muthukrishnan, J. Paulo Davim. Optimization of machining parameters of Al/SiC-MMC with ANOVA and ANN analysis. *Journal of materials processing technology*. 209, 2009, 225–232.
3. I. Singh, N. Bhatnagar, P. Viswanath. Drilling of uni-directional glass fiber reinforced plastics: Experimental and finite element study. *Materials and Design*. 29, 2008, 546-553.
4. C.C. Tsao, H. Hocheng. Evaluation of thrust force and surface roughness in drilling composite material using Taguchi analysis and neural network. *Journal of materials processing technology*. 203, 2008, 342–348.
5. Koenig W, Wulf C, Grass P, Willerscheid H. 1985. Machining of fiber reinforced plastics. *Manufact Tech CIRP Ann*. 34(2):537–48.
6. Miller JA. 1987. Drilling graphite/epoxy at Lockheed. *Am Mach Autom Manufact*. 70–1.
7. Lin SC, Chen IK. 1996. Drilling of carbon fiber-reinforced composite material at high speed. *Int J Mac Tools Manufact*. 156–62.
8. Piquet R, Ferret B, Lachaud F, Swider P. 2000. Experimental analysis of drilling damage in thin carbon/epoxy laminates using special drills. *Int J Mac Tools Manufact*. 1107–15.
9. Ugo Enemuoh E, Sherif El-Gizawy A, Chukwujekwu Okafor A. 2001. An approach for development of damage-free drilling of carbon fiber reinforced thermosets. *Int J Mac Tools Manufact*. 1795–814.
10. Yachida, M. and Tsuji, S. Industrial computer vision in Japan. *Computer*. 13, 1980, 50–63.
11. M. Kiran, B. Ramamoorthy and V. Radhakrishnan. Evaluation of surface roughness by vision system. *International Journal of Machine Tools & Manufacture*. 38(5), 1998, 685–690.
12. Du-Ming Tsai, Chi-Fong Tseng. Surface Roughness Classification for castings. *Pattern Recognition*. 32, 1999, 389-405.
13. M. Gupta and S. Raman. Machine vision assisted characterization of machined surfaces. *International Journal of Production Research*. 39(4), 2001, 759–784.

14. S.Y. Ho, K. Lee, S. Chen and S.J. Ho. Accurate modeling and prediction of surface roughness by computer vision in turning operations using an adaptive neuro–fuzzy inference system. *International Journal of Machine Tools & Manufacture*. 42, 2002, 1441–1446.
15. C.C. Tsao. Investigation into the effects of drilling parameters on delamination by various step-core drills. *Journal of materials processing technology*. 206, 2008, 405–411.
16. ISO 4288:1996. The rules and procedures for assessment of surface texture, International Organization for standardization, 1998, 1-30.

EXPERIMENTAL ANALYSIS OF SPOT WELD GROWTH ON CARBON STEELS USING PNEUMATICS-DRIVEN 75KVA SPOT WELDER

Nachimani Charde

Department of Mechanical, Material and Manufacturing Engineering,
Faculty of Engineering,
The University of Nottingham Malaysia Campus,
Jalan Broga, 43500 Semenyih, Selangor Darul Ehsan, Malaysia
Email: nachi.charde@nottingham.edu.my

ABSTRACT

Carbon steel is very common material that used in automotive industries for its supporting assembly always. So the joining mechanism of steels has to be low cost, reliable and last longer. In such situations the automotive industries are preferred to use the resistance spot welding techniques. The robustness of mechanical assemblies is mainly anticipated and it relies on the proper weld joint. Hence this paper is investigating the characteristics of carbon steel's weld joints with respect to its process parameters; primarily, the welding currents, welding durations or time cycles and electrode pressing forces. The entire experiment was carried out by varying the current and weld time at first set of attempts and the current and force at second set of attempts. The welding processes were monitored using additional instrumentation set up from which the process signals were captured for each and every single weld cycle with the aid of force, current and voltage transducers. Finally the welded samples were underwent mechanical and metallurgical tests to characterize the weld growth.

Keywords: Carbon steel, Carbon steel welding, Spot welding of steel

INTRODUCTION

Spot welding mechanism joins two or more metal sheets together through fusion. It is simply accomplished by compressing two copper electrodes on both sides of the base metals together and supplies huge amount of current (typically kA) through the contact areas of electrodes (Nachimani, C.

2011). The flow of current against the sum of resistive path that consists of electrodes to sheets resistances, bulk resistances and sheets to sheets resistances caused heat generation. The melt starts between the base metals due to highest resistances in the resistive path and gradually melts the asperity areas. Once the current flow is stopped then the molten area will be transformed into solid metal (Aravinthan et al., 2011). The melted and solidified areas of base metals are thereafter, called as weld nuggets and it consists of three major zones (Amuda et al., 2009). They are named as fusion zone (FZ), heat affected zone (HAZ) and base metals (BM). The proper joints between sheets are usually created by the fusion zones and their growths are related to the thermal expansion rate of materials. The surrounding areas of fusion zones are named as heat affected zones and it is partially affected by heat due to the thermal conductivity rate of base metals and the remaining part of base metals are unchanged (Bayraktar et al., 2006). The weld nuggets' growths are therefore determined by the process controlling parameters; primarily, the welding current, welding time, electrode pressing force and electrode tips diameter. These are the four common parameters that enable a weld growth but only the welding current, weld time and electrode force were varied to characterize the weld growth while electrode tip kept unchanged. The spot weld growths are however estimated from its nugget growth ($D=3\sqrt{t}$) and its bounding strength.

Moreover the other parameters such as resistive variations, resulting heat generations and the solidification processes are also concerned as important parameters to characterize the weld growth. Normally, when a welding process is functioning on, the resistive changes of the concerned area will generate equivalent heat changes ($Q = I^2Rt$) and consequently the high resistances areas will be melted. Thereafter it unites through liquidus stages of both sides of base metal and forms mechanical bonds once the solidification process is over.

EXPERIMENTATION

The base metals are rectangular in shape with 200 mm of length, 25 mm of width and 1 mm of thickness; as shown in figure 1. Its chemical properties are given as follow: C = 0.23, Fe = 98.05, Mn = 0.90, Si = 0.006, S = 0.05, P = 0.04

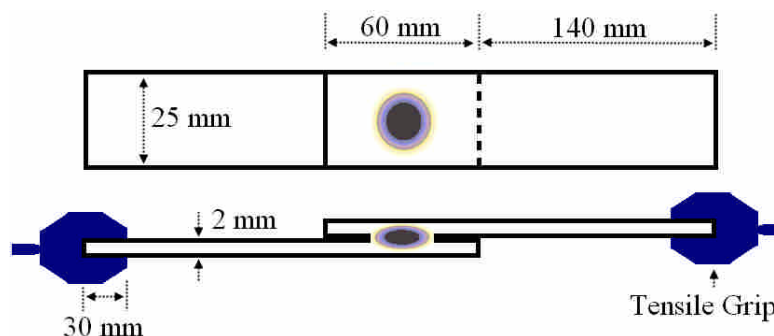


Figure 1. Test sample.

A pair of water cooled copper electrodes with truncated-tip diameters of 5 mm was used to join these base metals. The test samples were initially placed on the top of lower electrode (tip) of the spot welder as

overlying 60 mm on each other and then the initiating pedal was pressed. The weld process was started right after with squeezing cycles and; once the squeezing force is reached the welding current is delivered in accordance with the given preset values. Thereafter the electrode pressing mechanism (pneumatic based) consumes some time for cold work and eventually return to the home position of electrode. This is how the welding processes were done throughout of the entire experiments and the process controlling parameters (current, weld time and force) were set onto the controller before the welding process is started. Moreover some tests were conducted in advance to finalize the welding lobe (figure 2) for 1 mm base metals from which the welding schedule was laid out to complete the experiments.

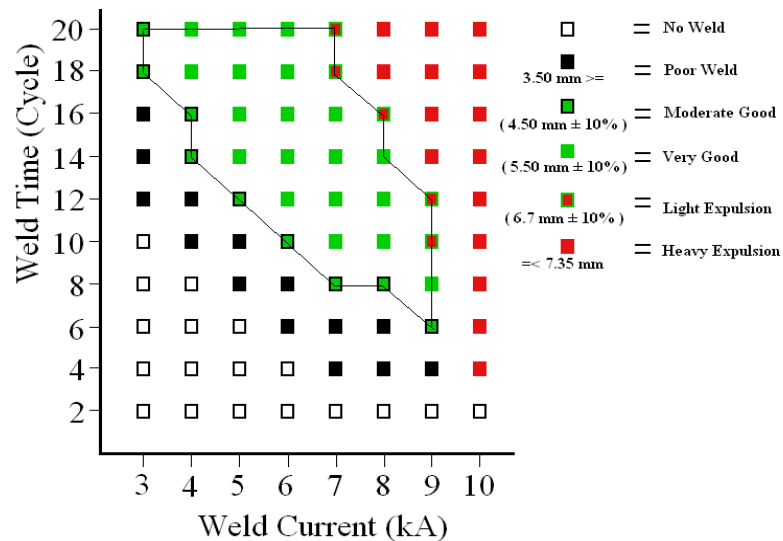


Figure 2(a). Welding lobes for 1mm sample sheets (Weld time versus welding current).

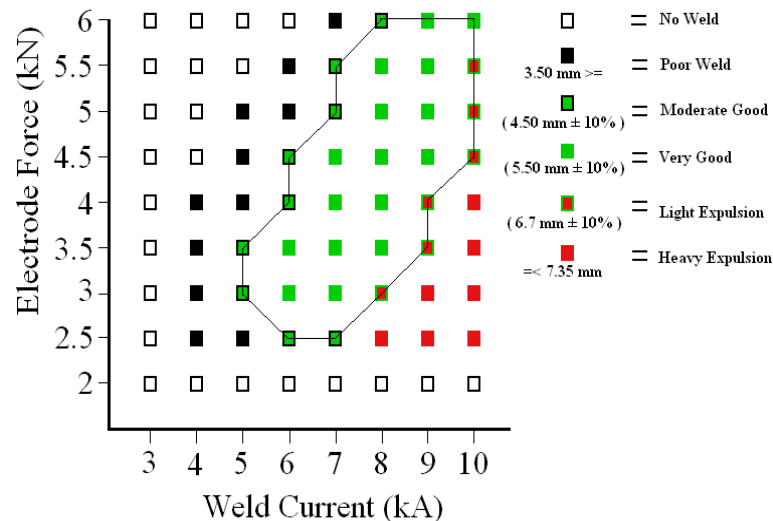


Figure 2(b). Welding lobes for 1mm sample sheets (Electrode force versus welding current).

Table 2. Weld schedule

Both	a) Current and	b) Current and
------	----------------	----------------

Sample no	Weld schedule	Electrode Tip (mm)	Current (kA)	weld time		force	
				Time (cycle)	Force (kN)	Time (cycle)	Force (kN)
1-5	1	5	6	10	3	10	3
6-10	2	5	7	10	3	10	3
11-15	3	5	8	10	3	10	3
16-20	4	5	6	15	3	10	4.5
21-25	5	5	7	15	3	10	4.5
26-30	6	5	8	15	3	10	4.5
31-35	7	5	6	20	3	10	6
36-40	8	5	7	20	3	10	6
41-45	9	5	8	20	3	10	6

A weld schedule was developed using the welding lobe (Figure 2(a and b)) to avoid expulsion and poor welding conditions. The welding conditions were limited to those lying within the lobe for the 1 mm metal sheets. So eighteen (18) weld schedules were developed and it has been shown in table 2. The first combination for the welding current against welding time with constant force and; the second combination for the welding current and electrode force with constant welding time. The weld lobe boundary indicated by continuous lines, delineates all acceptable welding conditions. The colored symbols represent the quality of welds and meanwhile, the conditions that did not produce welds are indicated by white boxes. The green colored boxes with black borders represent moderate to good welds; the fully green boxes represent very good welds; the red colored boxes bordered in green represent welds for which light expulsion occurred; the red boxes represent heavy expulsion and the black boxes represent poor weld joints. The selected welding parameters were equally spaced (7, 8, 9 kA; 10, 15, 20 cycle; and 3, 4.5, 6 kN) within the welding lobe to ensure full coverage of the welding conditions are sustained (Jamasri et al., 2011). The welded samples were subjected to tensile-shear tests as well as the hardness tests (Kent, P., 2000). The results of these two tests alone were insufficient to completely the characterization of weld growth. So a metallurgical study was carried out at last (Maa et al., 2008). While performing the entire welding processes, the electrical signals that of the welding current, terminal voltage and electrode force were captured using sensors, transducers, and crocodile clips. The captured signals were then sent through conditioning and amplifying circuits to data analyzing software (signal express 2010) to perform the final computation. Figure 3 shows the instrumentation set up for process parameters. This set up has managed to collect the voltage, current and force waveforms during the entire welding process (Marashi et al., 2008).

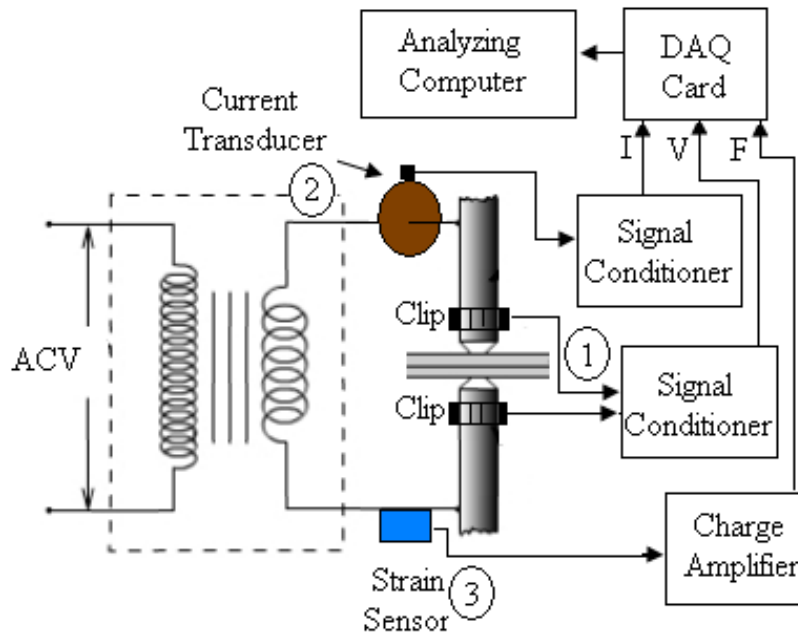


Figure 3. Instrumentation set up for the process parameters.

Figure 4 shows a typical force profile of pneumatic based spot welder for carbon steel. The squeezing profiles (1) are transient states in which the electrodes are pressing the base metals according to the preset values. Once it reaches the preset values, it holds the electrode firmly with that particular force thereafter. If the electrode pressing force is 3 kN, then the pneumatic system will press the electrode lever to produce 3 kN and the welding current will be released. The electrically generated forging forces (force increased in accordance with the welding current flow) will exist due to the force that helps the huge amount of current to pass through the base metal electrically.

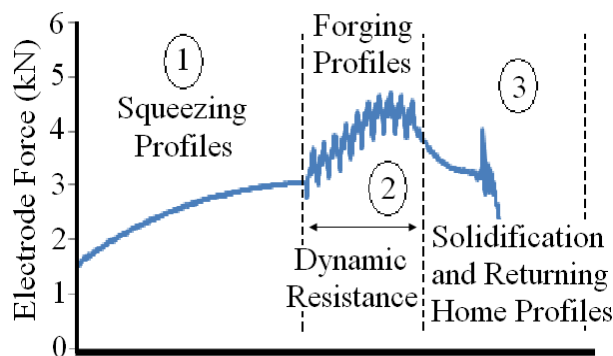


Figure 4. Typical force profile of pneumatic based spot welder for carbon steel.

Figure 5 and 6 are showing the root mean squared (rms) values of current and voltage waveforms that used to calculate the dynamic resistances. The dynamic resistance is calculated ($R=V/I$) for a period of 10 weld cycles.

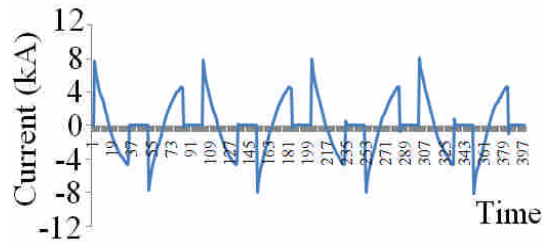


Figure 5. Current waveform from conditioning circuit.

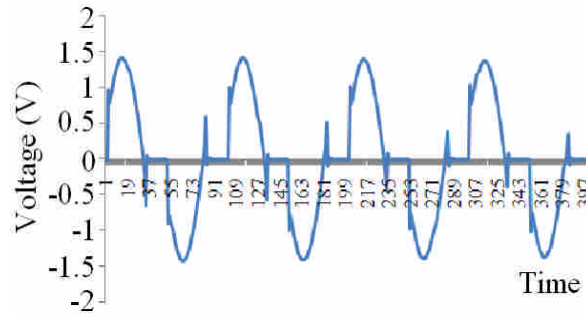


Figure 6. Voltage waveform from conditioning circuit.

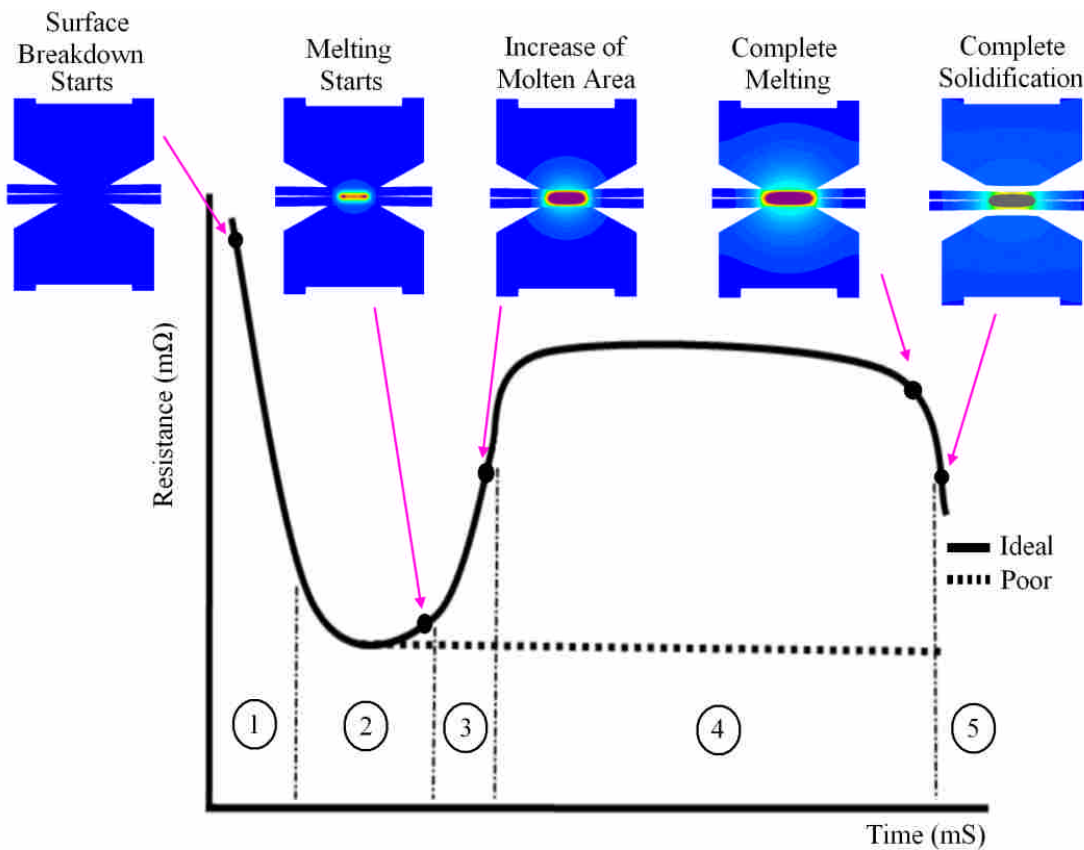


Figure 7. Dynamic resistance patterns.

Figure 7 shows the dynamic resistive pattern which was used to predict the process resistance during welding process for good and poor weld joints. So the entire dynamic resistive patterns are computed based on this referencing model using rms-current and rms-voltage waveform of 75kVA spot welder.

When considering the regions (1, 2, 3, 4 and 5) of figure 5, the region 1 reveals that the impurities on the surface of base metals cause high resistance between electrode tips and metal sheets during the initial current flow and also react as an insulator. As such sharp drops of resistances are found when a proper contact is established between electrode tip and metal sheet. The region 2 shows that the contact resistance of base metals is minimized in this region due to the presence of current flow. In another word: the contact areas that have to be welded are well balanced here and it acts as reference point to predict the expulsion states from here on. Likewise, the region 3 shows the thermal increment of bulk resistive components (metal resistance) to start the melt process which will initialize the nugget formation between faying surfaces of base metal. The following region was numbered as 4 and it finalizes the actual weld diameters. In this region the contact resistance is almost minimized and the temperature seemed to be about constant. Hence the growth of fusion zone (diameter) was clearly noticed during this stage. Furthermore the following region (region 5) does not fall in the welding process but in the solidification process. In this stage the liquid metal becomes solid; resulting micro structural changes. A sharp fall in this region or in the middle of earlier region reveals that an expulsion has occurred. A poor weld joint occurs due to the expulsion as it splash out the molten metal from the weld nuggets

RESULTS AND DISCUSSION

Force Profiles, Dynamic Resistances and Heat Distributions

The force profiles of carbon steels for various current increments (6, 7 and 8 kA) are shown in figure 8(a) and the equivalent dynamic resistances' changes are shown in figure 8(b). The dynamic resistance is calculated within the welding process duration and it can be seen from the sinusoidal type of current flow in force profiles.

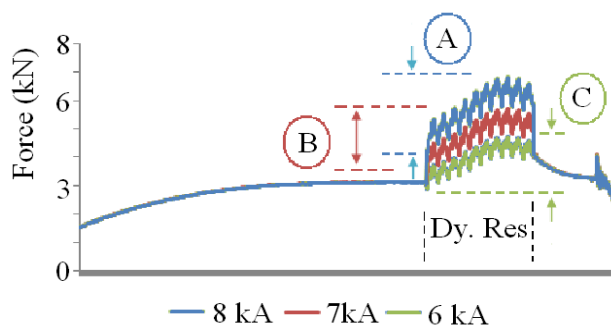


Figure 8(a). Force profiles of various current levels.

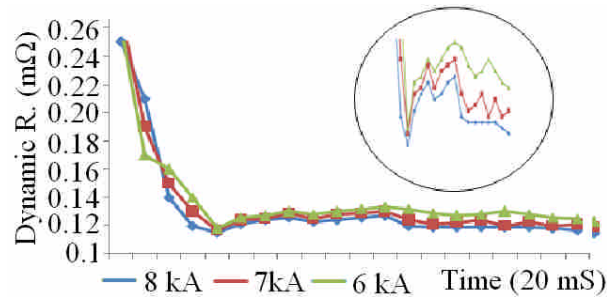


Figure 8(b). Dynamic resistances of various current levels.

These resistive patterns have been influencing the initial heat developments and also the heat distributions at the welding areas as shown in figure 8(c). This heat distributive pattern enables the nugget growth as it keeps melting the outer region (solid or HAZ) of molten areas; and this action goes simultaneously in all direction until the expulsion limit is reached. It was computed from the equation ($Q = I^2Rt$) as the weld time was 20 mS; current was 6, 7 and 8 kA; and resistance (R) was the dynamic resistive changes.

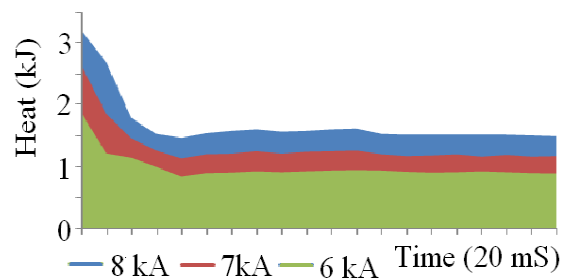


Figure 8(c). Heat generations of various current levels.

For example, when the current was increased from 6 to 7 and 7 to 8 kA; the dynamic resistances were slightly reduced but the initial heat developments and distributions were increased because of the multiplying factors of heat generation is made of time, resistance and current ($Q = I^2Rt$). Noticeably the drop of resistance in this case was minimal (mΩ) but the current increment was rapid enough; as it multiplies by itself (I^2) and therefore the heat was developed rapidly. In other words the current and heat increments were proportionally interrelated (figure 8(c)). When the starting heat was very high due to the static resistances, the melting was initially started at the middle of base metals (asperity) and growing outward in all directions (Shih et al., 2010). More specifically, the initial drops of resistances were seen at the beginning of dynamic resistive curves for all (6, 7 & 8 kA) due to the removal of surface contaminations and/or establish proper contacts with surfaces of base metals. Once the electrodes-to-sheets contacts' resistances are well balanced; the bulk resistances of base metals are started to accumulate the thermal increments on both metals sheets and the initial melt started at the contact areas of both metal sheets (asperity). When the melting temperature of the materials is reached at the asperities areas; the melting started immediately and therefore the heat travelled outward in all the direction with almost constant pattern of heat distribution which kept melting the contact area until the welding process is over (Guocheng et al., 2009). So this electrical resistivity and thermal conductivity is purely dependant

on the materials' properties and the diameters of molten areas are directly proportional with such heating effects (Li et al., 2011). According Dickinson's dynamic resistive model; the region 3, 4 and 5 are flatten in this experiments rather than bell-curve-like growth. These happened because of the forging force profiles of pneumatic based electrode actuation system and it has been minimized after the servo based system was implemented. Another situation was observed for the electrode pressing forces with constant current (6kA). The force was increased for few attempts and consequently the resistances were changed. When the electrode pressing forces from 3 to 4.5 and 4.5 to 6 kN were increased; the resistances were slightly decreased due to proper contacts between electrodes to sheets and such. These changes have resulted decrements in heat and the margin reduction among various forces were too narrow in heat distributions as compared to current increments. Figure 9(a), (b) and (c) show the various forces that applied; the equivalent resistive changes and resulting heat distributions on carbon steels, respectively.

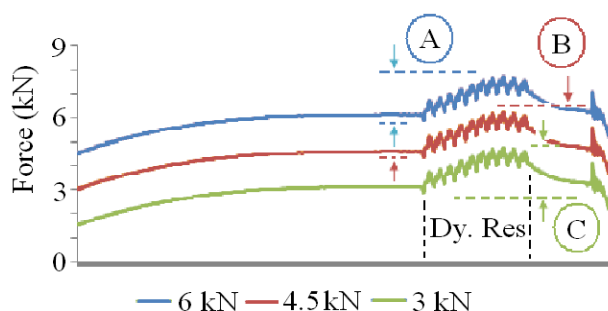


Figure 9(a). Force profiles of various force profiles.

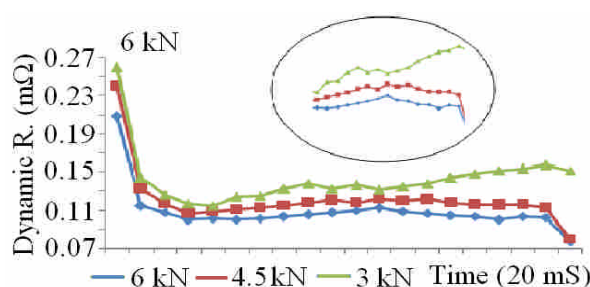


Figure 9(b). Dynamic resistances of various force profiles.

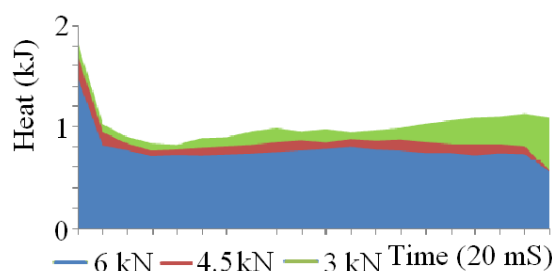


Figure 9(c). Heat generations of various force profiles.

Table 3 summarized the overall variation of electrically generated forging forces, dynamic resistances and also heat distributions according for the second set of experiments (welding current versus electrode force). Similar results were obtained when the welding time is increased for 15 and 20 weld cycles. By increasing the welding time to longer period; the heat distribution was noticed for longer period but other characteristics remained same. It is clearly seen from the table that the current increments caused huge amount of heat increments proportionally whereas the force increments caused drop of heat during welding process. The minimal and maximum values are listed to show the ranges of values noticed for these changes. Some researchers may curious why this effect is called as forging effects, at first place! The answer is simple and straight forward. When the heat and hammering effects are continuously or alternatively take place in spot welding process, the corresponding effects are actually forging effects in metal forming field.

Table 3. The electrically generated forging forces, dynamic resistances and heat distribution ranges.

	Various currents	8kA	7kA	6kA
Electrically Generated Forging Forces	Range (kN)	3	2.2	1.8
	Various forces	6kN	4.5kN	3kN
	Range (kJ)	2.2	2.1	1.8
	Various currents	8kA	7kA	6kA
Dynamic Resistance	Range (mΩ)	0.23 – 0.12	0.23 – 0.125	0.23 – 0.13
	Various forces	6kN	4.5kN	3kN
	Range (mΩ)	0.21 – 0.07	0.24 – 0.08	0.27 – 0.16
	Various currents	8kA	7kA	6kA
Heat Distribution	Range (kJ)	3.20 – 1.50	2.60 – 1.20	1.80 – 0.80
	Various forces	6kN	4.5kN	3kN
	Range (kJ)	1.45 – 0.58	1.68 – 0.58	1.80 – 1.10

Indentation of Welded Areas

The electrode pressing force was the root cause for the indentation at the area of concentrations (Khodabakhshi et al., 2011). This force creates a situation to splash out from the concerned areas when the nuggets' diameter grows beyond the electrode tips diameter which is always called as expulsion (Pouranvari, 2011a). However the worst case (expulsion) scenarios were not conducted in these experiments. Figure 10(a) shows the upper and lower indentation that created by electrode pressing force. Figure 10(b) shows the micro indentation that happened for both categories for parameters changes.

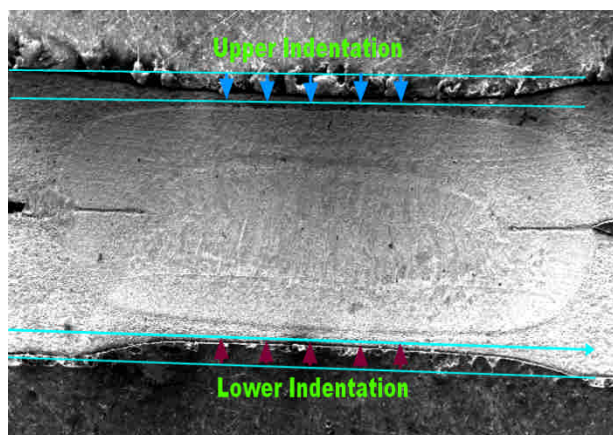


Figure 10(a). Indentation of welded area.

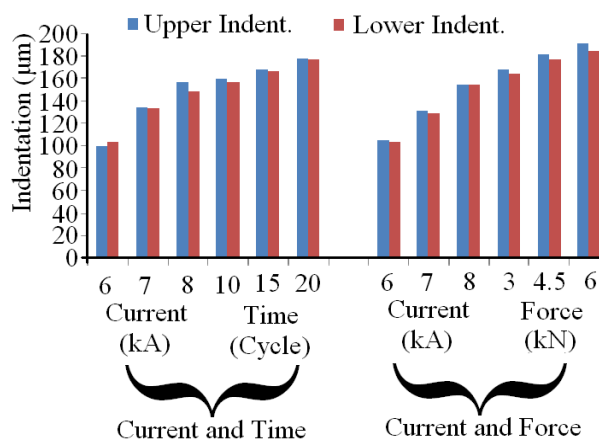


Figure 10(b). Indentation of the welded areas of both categories of welding conditions.

From the figure 10(b), it is obviously noticed that the indentation seemed to be proportional for all the three welding parameters (current, weld time and force). When there are increasing effects of welding parameters; the indentation goes deeper on both sides of base metals, then. In most cases the indentation was higher on upper electrode side because upper side was kept pressing by pneumatic cylinder during welding process. Although such electrode pressing force was applied during welding process, the electrically generated forging forces do exist due to the huge current flow from upper electrode through base metals to lower electrode and vice versa. When the input signal is sinusoidal; the direction of current flow is reversed according to different polarities of waveforms. This action happens few times at the

welded areas; following exactly the welding signal polarities and also for the duration of welding period. Figure 9(a) shows the typical force profiles for the carbon steel when forging forces happened. The demerit of the huge forging forces are that it helps the porosities to induced at the welded zones. Figure 11(a and b) show the porous that do exist for both category of welding conditions.

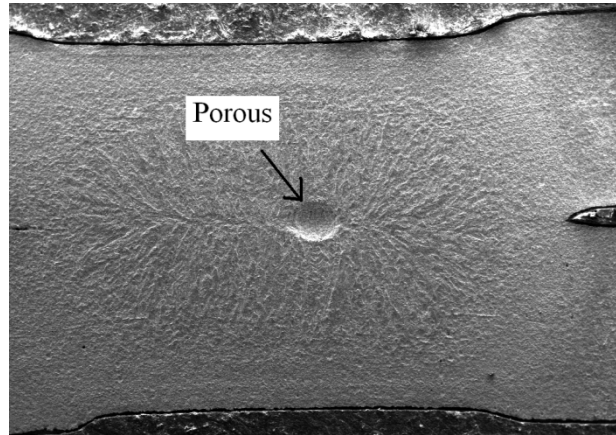


Figure 11(a). A porous existence at the welded zone due to huge forging forces.
(Welding time and welding current - category)

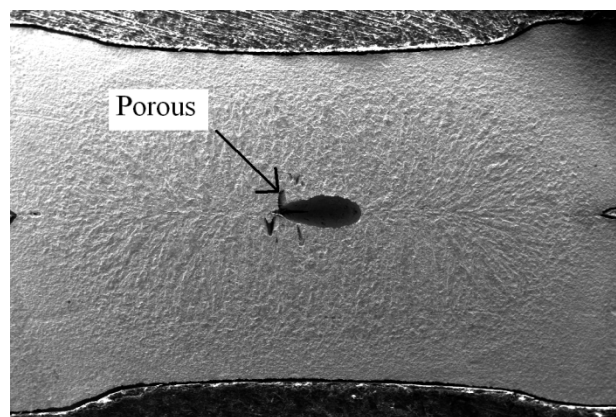


Figure 11(b). A porous existence at the welded zone due to huge forging forces
(Welding time and force - category).

Tensile Shear Test Results

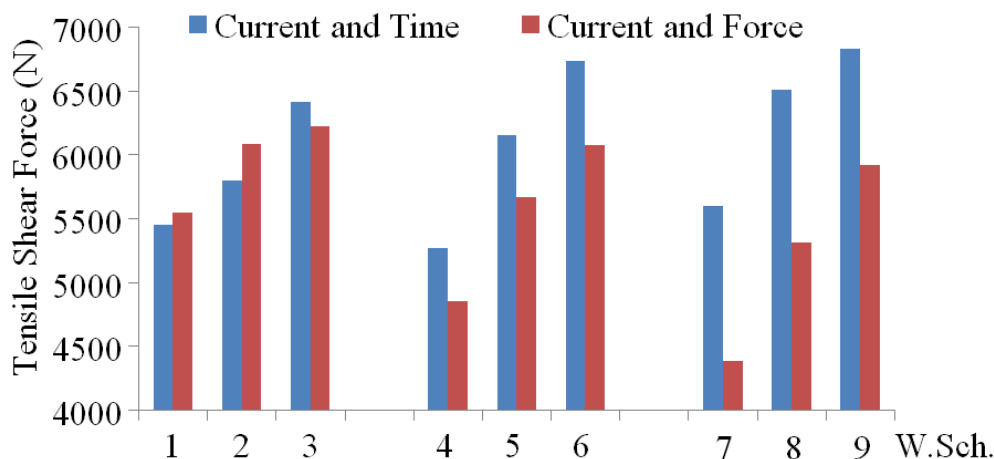


Figure 12. Tensile shear test results.

The tensile-shear test (Figure 12) was carried out using hundred kilo Newton (100 kN) capacity machine to determine the strength of spot welded samples of both ((current and weld time; current and force)) sets. The crosshead speed was maintained at 70 mm/min. The ultimate tensile strength (UTS) was taken as the maximum weld strength after which the weld joints have broken (Senkara and Zhang, 2004). Average strength values from the five samples were taken as the equivalent strength of that particular weld schedules. As for the weld schedules from 1 to 2 and 2 to 3 were analyzed; the strength increment was noticed due to the increment of welding current from 6 to 7 and 7 to 8 kA respectively. The similar increments were also noticed for the following weld schedules of 4, 5 and 6 as well as 7, 8, and 9. This obviously states that increase in current has caused increase in strength due to the increase in diameters. The Figure 13 shows the diameters changes with respect to current; weld time and force changes. These currents increment is found in both set of attempts. When the current and weld time incremental set is considered: the weld time too has increased the strength as it increases the diameters as well. This fulfils the Joule's law of heating ($Q = I^2Rt$); where Q represents the heat developed; I represents the current; R represent the resistance and t represent the time given. By increasing; either current or weld time; the heat supplied at the electrode tip is also equivalently increased and therefore the corresponding diameters increments were obtained. However when the current and force incremental set is considered: the force increase has caused drop in strength because of the drop of heat. As for the force from 3 to 4.5 and 4.5 to 6 kN; the tensile strength is reduced because the resistive components were reduced in the heating process which is another proportional coefficient of heat formula. Thus: the resistance is reduced by producing high electrode pressing force as it does changes in length (ℓ) which is a proportional coefficient of resistive equation. The bulk resistance is computed as $R = \rho \ell / A$; where ρ is the resistivity ($1.611 \times 10^{-7} \Omega.m$); ℓ is the length (1mm) and A is the contact area ($19.63 \mu m^2$) of electrode. The electrode tips were not changed at all so that the resistance is mainly affected due to changes in bulk resistance in addition to the contact resistances. Obviously, Figure 13 shows the drop of diameters when increase of force is concerned in this experiment. This phenomenon has also seen in the tensile test result by decreasing the diameter of weld nuggets.

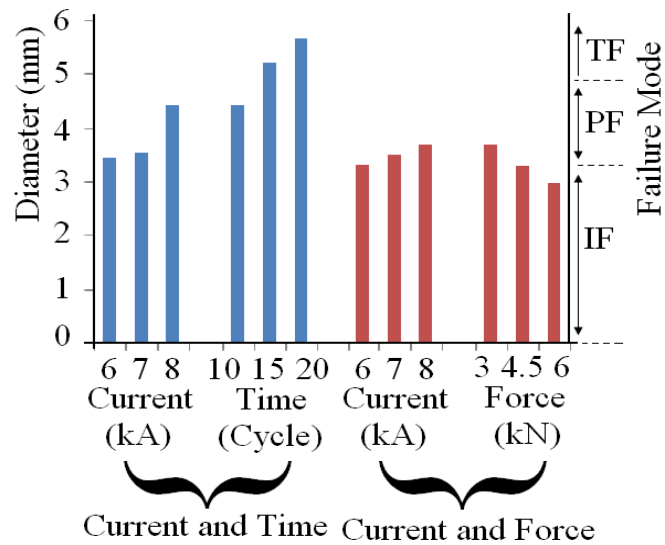


Figure 13. Diameter of weld nuggets and failure modes.

Failure Modes of Tensile Shear Tests

Having considered the failure modes of tensile test; we have noticed that the breaks happened in accordance with weld types (Darwish et al., 2004). A poor weld has interfacial fracture (IF) and the shear-force seemed to be falling between 4 to 5kN for 1mm base metals. A moderate-good weld has tear from either side of base metal (PF) and; the shear force falls between 5 to 6kN. Furthermore a good weld has better bounds between sheets and therefore it requires higher shear force to break the joints (6 to 7 kN). Often it tears from both sides and button pullout (TF) of the base metals as the break does not occur at the welded area but rather at the heat affected areas. Ever since the heat affected areas alters itself in hardness (slightly higher than base metals); both sides hold the welded areas firmly during tensile pulling to an extent where the tear trail enters the base metal regions and then breaks. Exact phenomenon was noticed by Bayraktar et al (2006). Figure 14(a) shows the failure modes with indicating points of IF, PF and TF while Figure 14(b, c and d) show the physical breaks as repetitive failures in groups (Pouranvari, 2011b).

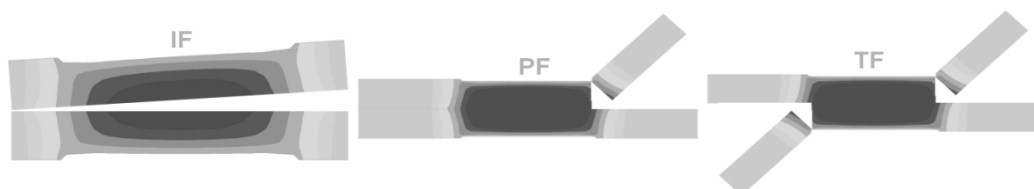


Figure 14(a). Failure modes.

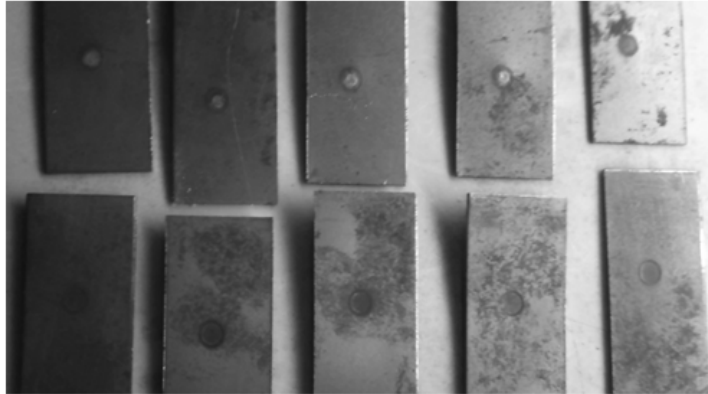


Figure 14(b). Interfacial failures (IF).



Figure 14(c). Tear from one side (PF) failures.

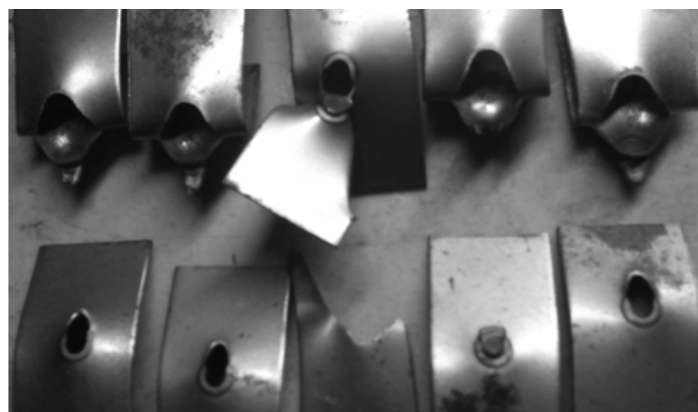


Figure 14(d). Tear from either side or button pullout (PF).

Metallurgical Study

The metallurgical test was conducted to view the micro and macro structural changes (Pouranvari et al., 2012a). Thus, such tests will easily help to predict the exact size of fusion and heat affected zones (Pouranvari et al., 2012b). A typical outlook of the fusion zones seemed to be coarse grains while the heat affected areas seemed to be finer grains regardless of controlling parameters changes. The parameters changes have directly influenced the grains at both: the fusion zones and the heat affected zones. Hence

the outlooks of such zones are varying from one macrograph to another. Further to this macrographs analysis for diameters, the micro structural zones were also measured for base metal, heat affected zone and fusion zone (Figure 15(a)). The base metals' micro structures have more pearlite and less ferrite in its region (Figure 15 (b)) as how it was made about with smaller grains as compare to the other two zones. The heat affected zones are transformed into martensite phases with some areas of pearlite and ferrite (Figure 15 (c)) with refined grains. However the fusion zones were seemed to be coarsened and larger in grain size as compare to the other two regions. This region had highest martensite formation with very few areas of pearlite nodules.

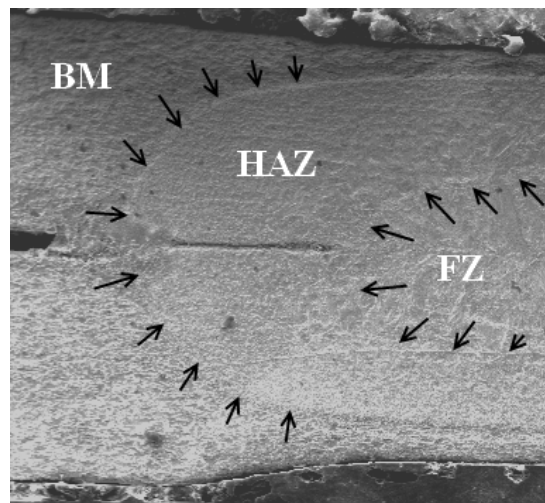


Figure 15(a). Structural zones.



Figure 15(b). Original grains matrix (BM).

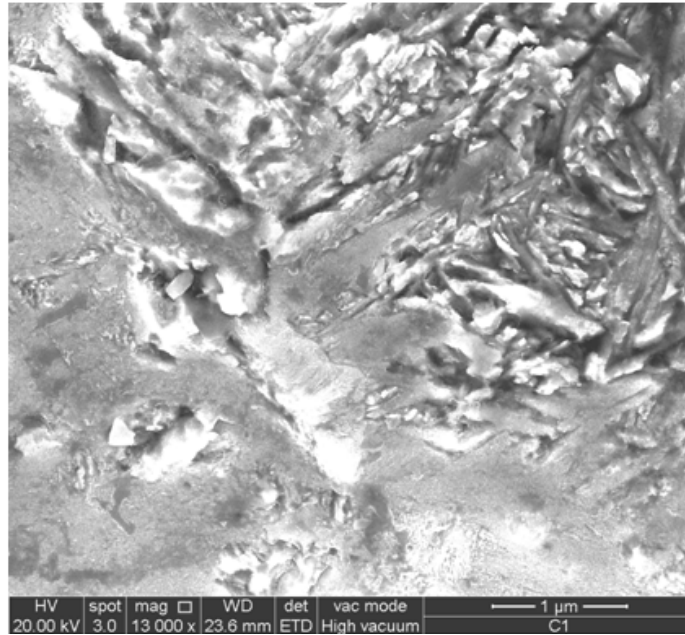


Figure 15(c). Refined grains matrix (HAZ).

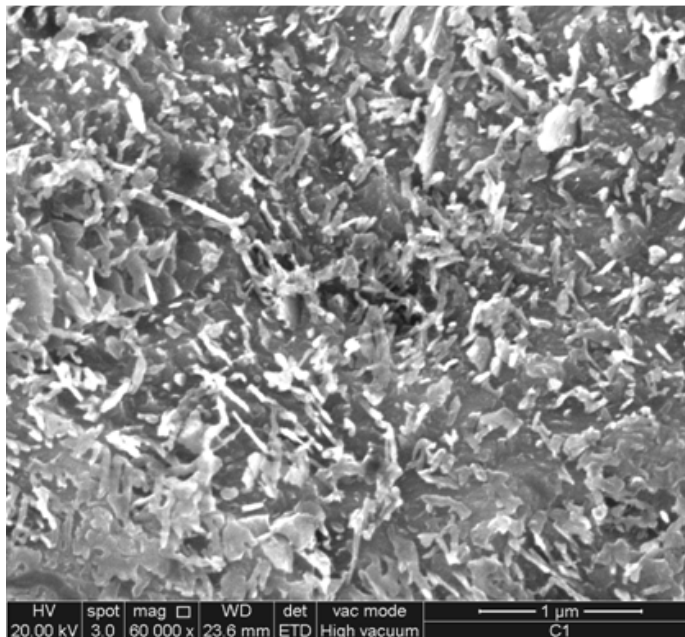


Figure 15(d). Grain coarsened matrix (BM).

Hardness Test Results

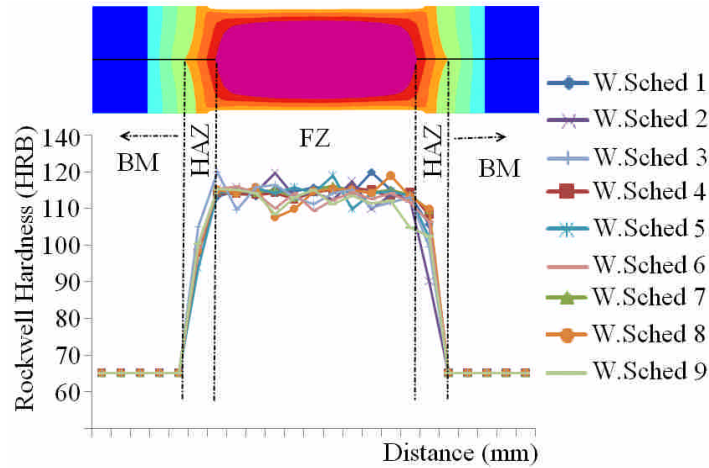


Figure 16(a). Hardness of carbon steels (Welding time vs. welding current).

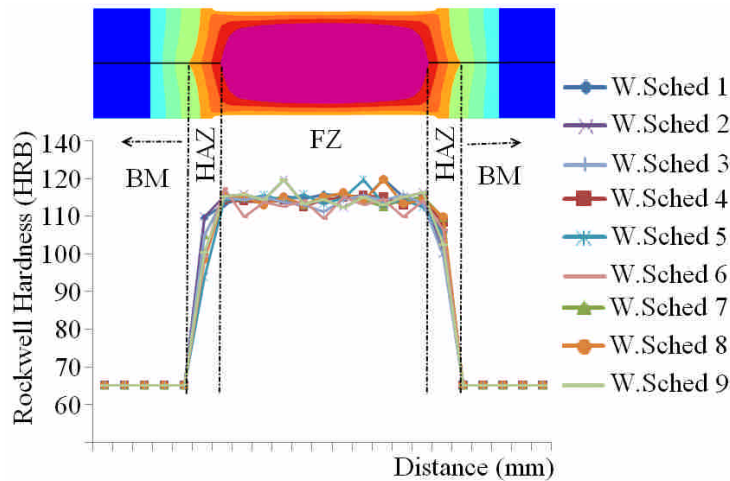


Figure 16(b). Hardness of carbon steels (Electrode force vs. welding current).

As for the hardness test the fusion zones (FZ) seemed to be symmetrical joints and oval shape was appeared (Gould et al., 2006). It has been hardened by the solidification process and the molten areas are directly related with thermal expansion's coefficient ($12 \times 10^{-6} \text{ K}^{-1}$). The heat affected zones' (HAZ) hardness was slightly lower than the fusion zone but higher than the base metals as how Kent et al (2008) was reported in his research. However the oval shape of heat affected zones was noticed because of the truncated electrodes tips and also the thermal conductivity ($54 \text{ W m}^{-1}\text{K}^{-1}$) of carbon steel. The hardness was measured for all the eighteen weld schedules as shown in figure 16(a and b). The hardness values of unwelded areas seemed to be 65 HRB whereas the fusion zones have produced around 115 HRB. However the heat affected zones have produced around 95 HRB approximately and fall between the base metal and the fusion zone.

CONCLUSIONS

This experimental paper looks into the spot weld nugget growth of carbon (0.3%) steel and it concludes that:

1. Increase in welding current (8kA) reduces the dynamic resistance as compared to 7 and 6 kA. However the heat generation is proportionally increased with respect to current increments ($Q = I^2Rt$).
2. Increase in electrode pressing forces have resulted decrement in dynamic resistances (3, 4.5 and 6kN); and therefore the decrement of heat was resulted.
3. The dynamic resistive pattern of D.W. Dickinson differed in this experiment because of the electrically generated forging forces' effects.
4. The micro indentation at the welded areas proportional to welding parameters (current, weld time and force).
5. The upper indentation seemed to be deeper because of the pneumatic force during welding.
6. The porosities exist not only for high current and long welding time but also for high forging force.
7. Increase in the welding current and welding time within the weld lobe have resulted increment in diameter of weld nuggets and therefore the increment of tensile strength was obtained.
8. Increase in electrode pressing forces have resulted decrement in diameter of weld nuggets and therefore the decrement of tensile strength was also obtained.
9. The common three failure modes were seen as poor weld produces interfacial fracture (IF); medium weld produces tear form one side (PF); and a good weld produces button pullout or tear from both sides (TF).
10. Micro structure exhibits that the coarsened grains at fusion zone, refined grains at heat affected zone and unchanged grains at base metal; clearly.
11. The hardness values of welded areas were increased (From 55 to 115 HRB in average) due to the nature of carbon steel. It happened due to the phase changes from moderate pearlite to most martensite.

ACKNOWLEDGMENTS

I would like to thank Ministry of Science, Technology and Innovation, Malaysia (MOSTI) for their financial support during the experiment. This research is extension of my PhD research work at Nottingham University Malaysia Campus.

References

- Amuda, M.O.H. and Mridha, S. 2009. Micro structural features of AISI 430 ferritic stainless steel (FSS) weld produced under varying process parameters. *International Journal of Mechanical and Materials Engineering*, Vol. 4, No. 2, 160-166.
- Aravinthan, A. and Nachimani, C. 2011. Analysis of spot weld growth on mild and stainless steel. *Welding Journal* August 2011: 143-147.
- Bayraktar, E., Moiron, J., and Kaplan, D. 2006. Effect of welding conditions on the formability characteristics of thin sheet steels: mechanical and metallurgical effects. *Journal of Materials Processing Technology*, 175, 20–26.
- Darwish, S.M., and Al-Samhan, A.M. 2004. Peel and shear strength of spot-welded and weld-bonded dissimilar thickness joints” *Journal of Materials Processing Technology* 147.
- Gould, S.P., Khurana and T. Li. 2006. Predictions of microstructures when welding automotive advanced high-strength steels. *Weld. Journal* 86: 111s–116s.
- Guocheng, X., Ling, W. and Chun, S.W., Xiaoqi, Z. 2009. Quality monitoring for resistance spot welding using dynamic signals. *Proceedings of the IEEE International Conference on Mechatronics and Automation*.
- Jamasri, Ilman, M.N., Soekrisno, R., and Triyono. 2011. Corrosion fatigue behaviour of RSW dissimilar metal welds between carbon steel and austenitic stainless steel with different thickness. *Procedia Engineering*, 10, 649-654.
- Kent, P., Von Maubeuge, and Henning E.N. 2000. Comparison of Peel Bond and Shear Tensile Test Methods for Needle Punched Geo Synthetic Clay Liners. *Geotextiles and Geomembranes*, 18, 203-214.
- Khodabakhshi, F., M. Kazeminezhad, Kokabi, A.H. 2011. Mechanical properties and microstructure of resistance spot welded severely deformed low carbon steel. *Materials Science and Engineering A*.
- Li, R.X. and Lei, X.C. 2011. Analyzing system of electric signals in spot welding process. *International Conference on Electronic and Mechanical Engineering and Information Technology* 2011.
- Maa, C., Chena, D.L., Bhole, S.D., Boudreau, G. Lee, A., and Biro, E. 2008. Microstructure and fracture characteristics of spot-welded DP600 steel. *Materials Science and Engineering A*, 485, 334–346.
- Marashi, P., Pouranvari, M., Amirabdollahian, S., Abedi A., and Goodarzi, M. 2008. Microstructure and failure behaviour of dissimilar resistance spot welds between low carbon galvanized and austenitic

stainless steels. *Materials Science and Engineering A*, 480 175–180.

Majid Pouranvari. 2011. Effect of Welding Parameters on the peak load and energy absorption of low-carbon steel resistance spot welds. *International Scholarly Research Network, ISRN Mechanical Engineering*.

Majid Pouranvari. 2011. Analysis of fracture mode of galvanized low carbon steel resistance spot welds. *International Journal of Multidisciplinary Science and Engineering*, Vol. 2, No. 6.

Majid Pouranvari, S. P. H. Marashi and S. M. Mousavizadeh. 2012. Dissimilar resistance spot welding of DP600 dual phase and AISI 1008 low carbon steels: correlation between weld microstructure and mechanical properties. *JMPT*.

Majid Pouranvari and S. P. H. Marashi. 2010. Key factors influencing mechanical performance of dual phase steel resistance spot welds. *Sci. Technol. Weld. Join.* 15, 149–155.

Nachimani, C. 2011. Spot weld growth on medium carbon steel (part 1), *International Journal of Mechanical and Materials Engineering* 243-247.

Senkara, S., Zhang, H and Hu, S. J. 2004. Expulsion prediction in resistance spot welding. *Welding Research*.

Shih, F.L, Li, X.W., Yoke R.W and Dong N.L. 2010. Input electrical impedance as quality monitoring signature for characterizing resistance spot welding. *NDT&E International* 43:200–205.

